Characteristics, Precursors, and Potential Predictability of Amu Darya Drought in an Earth System Model Large Ensemble

Andrew Hoell*[1], Jon Eischeid[1,2], Mathew Barlow[3], and Amy McNally[4]

[1]NOAA Physical Sciences Laboratory, Boulder, CO, USA

[2]Cooperative Institute for Research in the Environmental Sciences, University of Colorado Boulder, Boulder, CO, USA

[3]University of Massachusetts Lowell, Lowell, MA, USA

[4]NASA Goddard Space Flight Center, Greenbelt, MD, USA

* Andrew Hoell, NOAA Physical Sciences Laboratory, 325 Broadway, Boulder, CO, USA, email: andrew.hoell@noaa.gov

Abstract

The socioeconomic stability of the Central Asian Republics in the Amu Darya watershed is sensitive to drought. Activities related to agriculture employ a large fraction of the population and are responsible for at least one fifth of the gross domestic products of Afghanistan, Tajikistan, and Turkmenistan. Toward building a predictive understanding that may be applied to drought early warning practices, the characteristics, precursors and potential predictability of agricultural drought in the Amu Darya watershed are examined in a large ensemble of Community Earth System Model version 1 simulations during 1920-2019. Agricultural drought is examined over Upper and Lower regions of the Amu Darya watershed, which have different mean hydroclimates, and is defined by 1-m soil moisture deficits lasting three or more months.

The likelihood of drought onset and demise is phase-locked with the seasonal cycle of precipitation of each region, but with some notable differences. For the Upper region, drought onset and demise are three times more likely to occur during Autumn and Spring than other seasons. For the Lower region, drought onset and demise are three times more likely to occur during November-April than during Summer. Precipitation anomalies drive drought onset and demise during the climatological wet periods of both regions while temperatures play a smaller role. The probability of drought onset and demise is modulated by La Niña and El Niño, which control the interannual variability of precipitation over the Central Asian Republics during their wet seasons, indicating that the state of the El Niño Southern Oscillation serves as a key predictor of agricultural drought phase changes.

1. Introduction

1.1 Motivation

Rainfed and irrigated agriculture are key to the well-being of four Central Asia Republics in the Amu Darya watershed (Rakhmatullaev et al. 2010). Afghanistan, Tajikistan, Turkmenistan, and Uzbekistan (Fig. 1) generate 20.5%, 21.2%, 9.3% and 28.5% of their gross domestic product, respectively, from activities related to agriculture (The World Bank 2019a). The Central Asian Republics are therefore exceptionally sensitive to agricultural production shocks since they are among the world's poorest nations (The World Bank 2019b), the agricultural sector employs a large fraction of the population (Mirzabaev 2018), and food insecurity is already widespread (Food and Agricultural Organization of the United Nations 2018).

Drought is a key driver of shocks in agricultural production and the socioeconomic wellbeing of nations in the Amu Darya watershed. Drought in 2018 led to crisis levels of acute food insecurity over most of Afghanistan (Famine Early Warning Systems Network 2018), which was related to the displacement of hundreds of thousands of people (British Broadcasting Company 2018; Al Jazeera 2018). Drought in 2007 and 2008 over Afghanistan led to a major decline in wheat production (United States Department of Agriculture Foreign Agricultural Service 2008) and was related to social instability that empowered the Taliban (Gall 2008). A three-year drought spanning 1999-2001 over Afghanistan led to water scarcity, little crop production and extreme hardship (Bearak 2000). While long-term droughts like 1999-2001 and 2007-2008 are arguably more harmful because the impacts span multiple years, the effects of droughts lasting one year or less like in 2018 should not be understated. Surface water

availability varies by as much as 30% between pluvial and drought years, which has ramifications for both irrigated and rainfed agriculture (Pervez et al. 2014).

Motivated by the devastating effects of drought in Central Asia, we investigate the characteristics, precursors, and potential predictability of agricultural drought in the Amu Darya watershed. Our goal is to build a more complete understanding of drought over this region to establish a foundation from which we can predict them with skill. This predictive understanding in turn may be used for early warning of food and water insecurity to provide aid more effectively to societies in need.

1.2 Background

Previous research on Central and Western Asia drought has largely focused on the drivers of precipitation variability during the rainy season that spans November-April (see Barlow et al. 2016 and references therein). Given our focus area, we limit our background discussion to this extended cold season over the Amu Darya watershed, which has a smaller set of drivers than the larger Central and Western Asia region. Key drivers relevant to Amu Darya precipitation and the time scales over which they operate include the El Niño-Southern Oscillation (ENSO) on seasonal time scales and the Pacific Decadal Oscillation (PDO) on decadal time scales.

ENSO, the leading mode of tropical interannual variability, is related to the frequency of distinct weather types over Central Asia (Gerlitz et al. 2018) that results in cold season precipitation anomalies over Afghanistan, Tajikistan and southern portions of Uzbekistan and

Turkmenistan (Barlow et al. 2002; Mariotti 2007; Hoell and Funk 2013; Hoell et al. 2013; Hoell et al. 2014a; Hoell et al. 2014b; Hoell et al. 2017a; Hoell et al. 2017b; Rana et al. 2017; Hoell et al. 2018b; Rana et al 2017; Rana et al. 2018; Gerlitz et al. 2019). El Niño, the warm phase of ENSO, is on average related to above average precipitation over the region while La Niña, the cold phase of ENSO, is on average related to below average precipitation over the region.

Several characteristics of El Niño and La Niña events affect Amu Darya watershed precipitation. First, Amu Darya precipitation is sensitive to the flavor of a given ENSO event (Hoell et al. 2014a; Hoell et al. 2014b; Hoell et al. 2018b), where flavor refers to the longitudinal location of the strongest tropical Pacific sea surface temperature (SST) anomalies during El Niño or La Niña (e.g. Johnson 2013; Capotondi et al. 2014). Central Pacific La Niña events are related to a high probability of below average precipitation over the Amu Darya watershed while eastern Pacific La Niña events are not. Both eastern and central Pacific El Niño events are related to high probabilities of above average precipitation over the Amu Darya watershed. Second, Amu Darya precipitation is sensitive to the magnitude of SST anomalies in the western Pacific during La Niña events (Hoell and Funk 2013; Hoell et al. 2014a). The warmest west Pacific SSTs during La Niña events are related to the largest negative precipitation departures. Finally, the relationship between ENSO and Amu Darya precipitation changes in time (Hoell et al. 2017a; Rana et al. 2018), either because of differences in SST anomalies related to ENSO, internal atmospheric variability, or both.

SST patterns related to the PDO, the leading mode of decadal North Pacific SST variability (e.g. Zhang et al. 1997; Manuta et al. 1997; Newman et al. 2016), have been linked to extended cold season precipitation over the Amu Darya watershed (Hoell et al. 2015b; Rana et

al. 2019). SST patterns related to the positive phase of the PDO resemble El Niño and are associated with above average Amu Darya watershed precipitation. SST patterns related to the negative phase of the PDO resemble La Niña and are associated with below average Amu Darya watershed precipitation. Given that the SST patterns related to the PDO are a result of many processes, which include teleconnections related to ENSO and local atmosphere-ocean interactions over the North Pacific (Newman et al. 2016), it is unclear at this time whether the PDO itself drives Amu Darya precipitation or whether their relationship is a symptom of consecutive ENSO events.

A common theme among ENSO and PDO are their origins in the tropical Indian and Pacific Ocean. While some differences exist between them, both excite tropospheric convection and diabatic heating anomalies over the tropical Indian Ocean, Maritime Continent and west-central Pacific Ocean, which in turn force atmospheric circulation anomalies over the Amu Darya watershed (Barlow et al. 2002; Barlow et al. 2007; Hoell et al. 2013; Hoell et al. 2017b).

There are two known pathways through which the atmospheric circulation anomalies reach the Amu Darya watershed. The first, and most direct pathway, is through a Gill-Matsuno (Matsuno 1966; Gill 1980) response. In this response, baroclinic Rossby waves develop poleward and westward of the tropical diabatic heating anomalies over the Indian and Pacific Ocean (Barlow et al. 2002; Barlow et al. 2007; Hoell et al. 2013; Hoell et al. 2017b). The second pathway is through stationary Rossby waves with northeastward group velocity that make their way around the globe to the Amu Darya (Shaman and Tziperman 2005; Hoell et al. 2013; Niranjan Kumar et al. 2016). This second pathway has only been linked to ENSO, presumably because it requires forcing to be sustained over weeks to seasons.

120 The atmospheric circulation anomalies alter the local vertical motions and flux of
121 moisture, which in turn modifies Amu Darya precipitation. In terms of vertical motions, the
122 baroclinic Rossby waves interact with the mean jet, which produces anomalous temperature
123 advection that is subsequently balanced by precipitation-altering anomalous vertical motions
124 (Barlow et al. 2002; Barlow et al. 2007; Hoell et al. 2013; Hoell et al. 2017b; Hoell et al. 2018b).
125 In terms of atmospheric moisture fluxes, the atmospheric circulation anomalies lead to
126 precipitation-altering moisture flux convergence anomalies (Hoell et al. 2017b, Cannon et al.
127 2017, Hoell et al. 2018b)

128

129 1.3 Outline

130 Previous research related to Central Asia drought has largely focused on the behavior of
131 precipitation during the region's rainy season (see Barlow et al. 2016 and references therein).
132 Given that precipitation constitutes only part of the surface water budget, an understanding of
133 agricultural drought is lacking over the Amu Darya watershed. Here, we investigate agricultural
134 drought using variations in 1-m soil moisture (World Meteorological Organization 1975), since
135 soil moisture integrates the effects of supply (precipitation) and demand (potential
136 evapotranspiration) on the surface water balance.

137 Agricultural drought is examined using a 40-member ensemble of transient fully coupled
138 earth system model simulations during 1920-2019. The earth system model simulations are
139 based on the Community Earth System Model version 1 (CESM1) large ensemble from the
140 National Center for Atmospheric Research (Kay et al. 2015). The 4000 years of simulated

environmental conditions provides a large sample from which to probe drought behaviors than is possible from the existent observed record over the region that is spatially and temporally incomplete (Fig. 2; see also Hoell et al. 2015b and Hoell et al. 2017a). The earth system model, the estimates of observed conditions that are used to benchmark the model, and methods employed are described in sections 2 and 3.

In section 4, we probe the characteristics, precursors, and potential predictability of agricultural drought in the Amu Darya watershed. To better appreciate the variety of drought characteristics possible in the watershed, we begin with a discussion on the potential variability of the region's hydroclimate based on traces of 1-m soil moisture in the earth system model. The first characteristic that we examine is drought prevalence, taken here to be the amount of time spent in drought for every 100 years. The second drought characteristic that we examine is duration by probing he likelihood of droughts lasting more than a certain amount of time. We then turn our attention to the behaviors of drought onset and demise and their potential predictability by addressing the following questions. During what months are onset and demise most likely? What conditions, in terms of precipitation and air temperature and the lead times over which these conditions occur, are related to drought onset and demise? Are drought onset and demise related to phases of ENSO and are therefore potentially predictable? Are prolonged droughts related to persistent eastern Pacific SST anomalies?

2. Tools

2.1 Watersheds

The extent of the Amu Darya watershed is based on the HydroBASINS global watershed boundaries (Lehner and Grill 2013). HydroBASINS is constructed from the 'Hydrological data and maps based on Shuttle Elevation Derivatives at multiple Scales' (HydroSHEDS; Lehner et al. 2008) on a grid resolution of 15 arc seconds. HydroBASINS diagnoses a hierarchy of watersheds across 12 spatial scales, known as 'levels', that range in size from the continental scale (level 1) to the size of a lake with an area of less than 2 km^2 (level 12). Level 3 defines large river basins like the Amu Darya and level 4 defines the basins within large river basins. We therefore define the Amu Darya watershed based on HydroBASINS levels 3 and 4.

2.2 Climate Model Simulations

Two transient coupled climate model ensembles are considered. The first is comprised of 40 realizations of the CESM large ensemble version 1 (Kay et al. 2015). CESM1 is a sophisticated earth system model framework that is comprised of atmosphere (CAM5; Hurrell et al. 2013), land surface (CLM4; Lawrence et al. 2011), ocean (POP2; Smith et al. 2010) and sea ice components (CICE4; Hunke et al. 2013) all run at a nominal 1°x1° horizontal resolution. Each realization is forced by the same radiative forcing: historical forcing prior to 2005 based on Lamarque et al. (2010) and representative concentration pathway 8.5 (RCP8.5) forcing is applied thereafter based on Meinshausen et al. (2011) and Lamarque et al. (2011). While the same external forcing is applied to all 40 CESM1 realizations, each realization follows a different trajectory because of their initializations from slightly different atmospheric states. Differences between the CESM1 realizations are therefore a result of only internal variability of the earth

system (Kay et al. 2015). The second ensemble is comprised of a single transient realization of 37 different models listed in Table 1 that participated in the Coupled Model Intercomparison Project Phase 5 (CMIP5; Taylor et al. 2012). The external forcing of the CMIP5 models are like the CESM1 large ensemble. However, the architecture of each CMIP5 model are different as well as how and each of the models handle chemistry, radiative effects, and land surface changes.

2.3 Historical Precipitation, Temperature, and 1-m Soil Moisture Estimates

Gridded analyses of monthly precipitation, near-surface air temperature and 1-m soil moisture are used to diagnose estimates of observed conditions for comparison with climate models. Precipitation is based on the Global Precipitation Climatology Centre (GPCC, Schneider et al 2014) version 7 at a 1.0°x1.0° horizontal resolution. GPCC is constructed by combining monthly precipitation anomalies based on quality-controlled station data with a monthly climatology. The observed precipitation gauge network over Central and Southwest Asia common to all long-term historical precipitation reconstructions is sparse in space and time, particularly prior to 1950 and after 1990 (Fig. 2). Even during the three decades spanning 1960-1990 in which precipitation sampling was at its greatest in the Amu Darya, sampling in neither Upper nor Lower regions exceeded, on average, more than 0.5 stations per grid point in the GPCC precipitation dataset.

Near-surface air temperature is based on the terrestrial temperature dataset from the University of Delaware (UDEL; Willmott and Matsuura 2001) version 5.01 at a 0.5°x0.5°

204 horizontal resolution. UDEL is constructed by spatially interpolating available weather station
205 data from a suite of archives, which includes the Global Historical Climatology Network (Menne
206 et al. 2018) among others.

207 1-m soil moisture is based on a simulation of the CLM2 land surface model forced by an
208 estimate of the time-varying meteorology as part of the Global Land Data Assimilation System
209 (GLDAS; Rodell et al. 2004). Data from 1979-2019 on a 1°x1° horizontal grid with 10 vertical
210 levels, with the first seven reaching a depth of approximately 1m, is used. The CLM2 model is
211 analyzed because it is the predecessor to the CLM4 land model, the land component of CESM1.
212 Like estimates of observed precipitation, caution should be used when considering estimates of
213 GLDAS soil moisture in the Amu Darya watershed because the precipitation data used to force
214 the land surface models are not based on a spatially and temporally complete in situ data
215 (Fig.2; Hoell et al. 2015b; Hoell et al. 2017a).

216 Estimates of observed SSTs are based on the Extended Reconstructed Sea Surface
217 Temperature dataset version 5 (ERSST5; Huang et al. 2017). Observed SST estimates are used to
218 calculate the Niño3.4 index, area averaged SST anomalies over 5°S-5°N and 170°W-120°W, from
219 1920-2019.

220

221 **3. Methods**

222 3.1 Defining Upper and Lower Amu Darya Regions

The Amu Darya watershed is generally separated into Upper and Lower regions based on orography and hydroclimatic variability, as described by Rakhmatullaev et al. (2010). The Upper region, comprising the southeastern part of the watershed, is characterized by the complex orography of the Pamir and Hindu Kush mountains. The Lower region, comprising the northwestern part of the watershed, is characterized by lower elevation semi-arid steppe.

We separate the Amu Darya watershed similarly. The entire Amu Darya watershed, as indicated by the perimeter of the heavy polygons in Fig. 1b, is based on HydroBASINS level 3. An aggregation of many HydroBASINS level 4, as indicated by the light polygons in Fig. 1b, is used to define the Upper and Lower Amu Darya regions. The Upper region is comprised of three level 4 basins, which cover all of Tajikistan, northern Afghanistan, eastern Turkmenistan, and southern Uzbekistan. The Lower region is comprised of many level 4 basins, covering most of Uzbekistan, a small portion of eastern Turkmenistan and a tiny portion of southern Kazakhstan. Conditions over the Upper and Lower Amu Darya regions are based on area-weighted averages of the gridded data. For a grid box to be included in a regional average then 50% of its area must fall within the polygons that define the Upper and Lower Amu Darya.

3.2 Characterizing Amu Darya Hydroclimate Using Climate Models

Given the short and spatially incomplete existent observed record in the Amu Darya watershed (Fig. 2; see also Hoell et al. 2015b and Hoell et al. 2017a), we explore the suitability of two large ensembles of climate model simulations to probe drought behavior in the region. The first ensemble is comprised of a single simulation from many different CMIP5 models,

244 which has the advantage of not being biased towards a single model's architecture. The second
245 ensemble is comprised of many realizations from a single model, CESM1, which has the
246 advantage of sampling internal climate variability (according to that model) without confusing it
247 with differences in model architecture (e.g. Tebaldi et al. 2011, Kay et al. 2015).

248 A large ensemble comprised of many different CMIP5 models is not feasible for probing
249 drought over the Amu Darya watershed, given the great disparity among the CMIP5 models in
250 their ability reproduce key aspects of Upper and Lower region hydroclimate. Most models
251 cannot reasonably reproduce the precipitation seasonality and magnitude of monthly
252 precipitation when compared with estimates of observed conditions in the Upper and Lower
253 regions during 1920-2019 (Fig. 3). Especially noteworthy is that almost all CMIP5 models
254 simulate noteworthy precipitation into late spring and early summer when observed estimates
255 indicate that the climatological dry season has long begun. Most of the CMIP5 models simply
256 cannot be trusted in terms of representing reasonable drought behavior when the precipitation
257 seasonality is so erroneous.

258 By contrast, CESM1 is an example of a model that reasonably captures key aspects of
259 climatological precipitation in the Upper and Lower Amu Darya regions when compared with
260 observed estimates during 1920-2019 (Fig. 3), which provides some evidence that a large
261 ensemble of simulations based on this model may be suitable for probing drought over the
262 Amu Darya watershed. All 40 100-year CESM1 realizations capture the seasonal cycle well,
263 especially the increase in average precipitation from fall to winter and the decrease in average
264 precipitation from spring into summer. It is important to note, however, that CESM1 simulates

too much precipitation over the Upper region in late winter and early spring and too little precipitation over the Lower region during the core of the rainy season.

We further examine the suitability of CESM1 in representing Amu Darya hydroclimate by comparing box plots of monthly precipitation, 2-m air temperature and 1-m soil moisture with observed estimates (Fig. 4). As noted previously, similar seasonal cycles and spread of monthly precipitation are also found in the observed estimates and CESM1 for the Upper and Lower Amu Darya regions (Figs. 3 and 4). The rainy season for both regions spans November-April, though the specifics of the seasonal cycle are different between the two. Upper region precipitation peaks in February-April while Lower region precipitation is more evenly distributed across all months of the rainy season. CESM1 is wetter over the Upper region during spring and slightly drier over the Lower region when compared with observed estimates. Monthly precipitation variability is large for both the Upper and Lower Amu Darya regions in the observed estimates and CESM1, as demonstrated by the large spread in possible precipitation outcomes relative to the median, indicating a propensity for similar magnitudes of wet and dry extremes.

Likewise, similar 2-m temperature variability and seasonal cycles are found in the observed estimates and CESM1 realizations for the Upper and Lower Amu Darya regions (Fig. 4). Temperatures over both regions reach minimums during January and maximums during July, though the Upper region is colder during all months because of elevation. There are some biases in CESM's representation of 2-m temperature for both regions. Over the Upper region, there is a seasonality to the bias, as the model is colder during the cold season and warmer

286 during the warm season. Over the Lower region, the model is biased warm during the warm
287 season.

288 Furthermore, aspects of 1-m soil moisture behavior in observed estimates and CESM1
289 are similar over both Upper and Lower Amu Darya regions, particularly their seasonal cycles
290 (Fig. 4). Though this provides another line of evidence that CESM1 can simulate many aspects of
291 Amu Darya watershed hydroclimate, it should be noted that there is a disparity between the
292 values of CESM1 and CLM2-derived observed estimate of 1-m soil moisture. It's not entirely
293 clear how to interpret these differences, or whether these differences are meaningful, since the
294 CLM2 simulation uses a predecessor, not the same, land surface model as CESM1 and the
295 precipitation used to force the CLM2 simulation lack much in situ data after 2000 (Hoell et al.
296 2015b; Hoell et al. 2017a).

297 CESM1 also reasonably captures annual average observed precipitation estimates
298 spatially across the topographically diverse region (Fig. 1b), as similar patterns and magnitudes
299 of mean annual precipitation over the Amu Darya watershed are found (Fig. 5). The greatest
300 precipitation falls in the Upper Amu Darya region collocated with the Hindu Kush Mountains in
301 Afghanistan and the Pamir Mountains in Tajikistan. It must be noted that precipitation totals
302 are about 20% larger in the earth system model than in the observed estimates over these
303 elevated areas. Comparably lower annual precipitation is found in the Lower Amu Darya region,
304 with similar magnitudes and patterns between CESM1 and observations.

305 Perhaps most importantly, CESM1 appears to capture a realistic relationship between
306 Amu Darya precipitation and ENSO during the region's wintertime rainy season. This is a

307 necessary characteristic of an earth system model used to diagnose weather and climate in the
308 Amu Darya watershed, given the known sensitivity of Central and Southwest Asia to El Niño and
309 La Niña events. Like Hoell et al. (2017a), a realistic precipitation response to ENSO simulated by
310 CESM1 is demonstrated by comparing 30-year end point correlations of the Niño3.4 index and
311 precipitation between the 40 CESM1 realizations (Fig. 6, gray lines) and the observed estimates
312 (Fig. 6, pink line) during November-April. For correlations ending after 1970, the 30-year period
313 in which observations in the regions increase (Fig. 2), the observed estimates fall within the
314 spread of the 40 CESM1 ensemble members. It is important to note, however, that the 30-year
315 correlations based on observed estimates falls on the low end of the CESM1 realizations before
316 2000. If the observed precipitation estimates are to be trusted, then these correlations may
317 suggest that the Amu Darya sensitivity to ENSO may be marginally too strong in CESM1.
318 Moreover, since observed estimates are analogous to a single realization of a climate model,
319 we highlight that the correlations based on observed estimates (Fig. 6, pink line) display similar
320 properties as a single trace of CESM1 (Fig. 6, orange line) in terms of decadal fluctuations,
321 further suggesting the realism of the model.

322 Based on the comparison of key hydroclimatic variables simulated by CESM1 with
323 observed estimates (Figs. 3-5) and CESM1's apparently ability to capture a realistic ENSO
324 response (Fig. 6), we employ the 40-member ensemble of CESM1 simulations to diagnose
325 drought over the Upper and Lower Amu Darya watershed. While Amu Darya drought
326 characteristics would be subject to possible biases of CESM1, we argue that a large ensemble
327 based on this earth system model is the best tool available to perform such a study, given the
328 inability of most CMIP5 models to realistically simulate key climatic aspects in this region (Fig.

329 3). Furthermore, using a large ensemble of CESM1 ensures that internal climate variability in
330 the model may be sampled without confusing it with differences in model architecture (e.g.
331 Tebaldi et al. 2011, Kay et al. 2015).

332

333 3.3 Defining Drought

334 Given the importance of widespread crop production over the Upper and Lower Amu
335 Darya regions, we focus on agricultural drought, defined by the World Meteorological
336 Organization (1975) as "the degree to which growing plants have been adversely affected by an
337 abnormal moisture deficiency." Our definition of an agricultural drought-related moisture
338 deficiency is based on 1-m soil moisture percentile ranks from the CESM simulations. Our
339 definition follows Keyantash and Dracup (2002) who found that agricultural drought is best
340 estimated by soil moisture computed in numerical models that consider a full water balance.

341 Droughts are identified separately in CESM1 for the Upper and Lower Amu Darya
342 regions. Drought for both regions occur when regionally averaged 1-m soil moisture falls below
343 the 20th percentile for 3 months or more and ends when soil moisture exceeds the 30th
344 percentile. This drought definition resembles Mo (2011) and Svoboda (2002), the latter of
345 which serves as the foundation for the U.S. Drought Monitor[1]. The definition of drought is
346 illustrated in Fig. 7 using 1-m soil moisture from the Lower Amu Darya in a single CESM1
347 realization. In this example, drought onset occurs in March 1982 and drought demise occurs in

[1] https://droughtmonitor.unl.edu/AboutUSDM/WhatIsTheUSDM.aspx

December 1982. There are 1200 drought events in the Upper and 851 drought events in the Lower Amu Darya regions in the 4000 simulated CESM years.

Monthly 1-m soil moisture, precipitation, 2-m temperature and SST variations are displayed as percentile ranks, as is common in the dissemination of seasonal forecasts from sources that include the World Meteorological Organization Global Producing Centres (https://www.wmolc.org/). A percentile rank for a given month is calculated against all like months in the entire ensemble of CESM1. For example, the percentile rank for any given March is calculated against all 4000 Marchs (the product of 40 realizations each 100 years in length). Conditions are above or below average when they rank in the upper and lower thirds of the record.

4. Results

4.1 Drought Characteristics and Variability

The behavior of 1-m soil moisture in each of the CESM1 realizations (Fig. 8) highlights the potential variability of the region's hydroclimate and emphasizes that agricultural droughts with a variety of characteristics are possible (Fig. 9). Given the differences in 1-m soil moisture variability among the 40 realizations, one could gain quite different perceptions of Amu Darya watershed drought, since each of the realizations is equally likely to occur. This also applies to the interpretation of an observed time series since that time series is analogous to a single model realization. In support of these points, behaviors of 1-m soil moisture are illustrated using the Lower Amu Darya region in Fig. 8. Similar features and the interpretation of those

features are gleaned from Upper Amu Darya region, which is not shown here in the interest of brevity.

Two examples of how 1-m soil moisture can vary in time in the Lower Amu Darya region are highlighted by pink and orange traces in Fig. 8. These two realizations of CESM1 were chosen because they have the greatest and fewest number of years in drought of the 40 simulations and they demonstrate a variety of 1-m soil moisture variability across time scales. The pink trace stands out as having high 1-m soil moisture percentiles throughout much of the 100-year period. Extended pluvial periods prevail, most notably during the 1920s, the 15-year period beginning in 1935, the 1960s and late 1990s. The post-2005 period was the driest time for the pink trace, as several one-year droughts emerged and quickly decayed. By contrast, the orange trace stands out as having low 1-m soil moisture percentiles throughout much of the 100-year period. Extended drought periods prevail, most notably during the 1930s, early 1940s, early 1960s and the post-2000 period. The orange trace was not without pluvial periods, however, as the late 1950s, early 1960s and early 1990s were a wet time in this realization.

Another key feature of 1-m soil moisture in the Lower Amu Darya region is the lack of long-term trend in the CESM1 ensemble average (Fig. 8, black line), which suggests that anthropogenic influences does not force aridification or wetting of the Amu Darya watershed in the earth system model for 1920-2019. The same result is found in Upper Amu Darya region. The average 1-m soil moisture across all simulations mutes the transient variability in each realization, thereby isolating the common feature among the simulations, which is the change in atmospheric composition and aerosols based on the CMIP5 protocol that is meant to replicate human influences. This result should not be interpreted as anthropogenic influences

391 cannot affect aspects of Amu Darya hydroclimate, but if there are effects, they are not manifest
392 in terms of changes in 1-m soil moisture in this ensemble of simulations.

393 Given the differences in 1-m soil moisture variability between each of the 40 CESM1
394 realizations (Fig. 8), we explore the possibilities in agricultural drought prevalence during 100-
395 year periods in the Amu Darya watershed (Fig. 9a). We find that both the Upper and Lower
396 regions demonstrate similarly large possibilities in the prevalence of drought in 100-year
397 periods, ranging from just a couple of years to as many as four decades . The large spread in
398 possible drought prevalence suggests potential pitfalls in anticipating drought prevalence at
399 future time horizons. Though not likely outcomes, droughts can prevail for as few as 8 years or
400 as many as 40 years in a 100-year period over the Lower Amu Darya. Likewise, droughts can
401 prevail for a few as 9 years or as many as 36 years in a 100-year period over the Upper Amu
402 Darya. While the unlikely tail values paint an extremely variable picture of drought prevalence
403 over the Amu Darya Watershed, there is still appreciable spread in the more likely outcomes.
404 The interquartile range of drought prevalence in 100-year periods for the Upper and Lower
405 regions spans approximately 18-27 years, a 9-year range that is about 40% of the median value
406 of 22 years.

407 We also probe the likelihood of drought length based on the 1200 and 851 droughts in
408 the Amu Darya watershed, respectively (Fig. 9b). There is a clear preference for short droughts
409 over the region, as 50% of droughts in both the Upper and Lower regions persist for less than
410 six and nine months, respectively. Continuing this preference, 75% of droughts in the Upper
411 and Lower regions persist for 12 months and 14 months, respectively. These results suggest
412 that droughts are rather frequent in the region and most are ameliorated in the rainy season

following drought onset. Despite this preference for droughts lasting a calendar year or less, CESM1 indicates that Amu Darya droughts in the upper quintile of the distribution can last for upwards of two years, as the top quintile of droughts in the Upper and Lower regions persist for 1.5 and 2 years, respectively. Most strikingly, the maximum drought length in the Upper and Lower regions in the earth system model simulations is 5 and 10 years, respectively.

4.2 Drought Seasonality, Precursors, and Potential Predictability

The occurrence of drought onset in the Upper and Lower Amu Darya regions, based on the median and interdecile range of occurrence from the 40 CESM1 realizations, demonstrates a distinct seasonality and a notable spread around the central value (Fig. 10). The seasonality of drought onset occurrence coincides with the precipitation seasonal cycle, but with some notable differences, and can vary greatly from one 100-year realization of the earth system model to the next. The variability among the realizations, obtained via the interdecile range, indicates that a single 100-year time series may not accurately reflect the most likely seasonality of drought onset occurrence.

In the Upper Amu Darya, drought onset occurrence is largest during the beginning of the rainy season, in November and December, and during the end of the rainy season, in March-May (Fig. 10a). While January and February make up the midst of the rainy season of the Upper region, the occurrence of onset during these months is about half as during the core months and is on par with the occurrence of drought onset during the June-October dry season. In the Lower Amu Darya, the occurrence of drought onset is approximately the same across all

434 months of the November-April rainy season, though it should be noted that the occurrence is
435 higher during December than the other months (Fig. 10c). The occurrence of drought onset
436 during the May-October dry season is rather low and is approximately a third of the occurrence
437 as during the rainy season.

438 Likewise, the occurrence of drought demise in the Upper and Lower Amu Darya regions
439 demonstrates a distinct seasonality that coincides with the precipitation seasonal cycle and a
440 notable spread around the central value (Fig. 10b,d). In the Upper Amu Darya, drought demise
441 occurrence is bimodal, with peaks during the beginning of the rainy season (October-
442 December) and the end of the rainy season (March-April). While January makes up the midst of
443 the rainy season in the Upper region, the occurrence of drought demise is less than half as in
444 fall and spring and is on par with some summertime months. In the Lower Amu Darya, the
445 occurrence of drought onset is approximately the same across all months of the November-
446 April rainy season, with a slight peak in November and December. The occurrence of drought
447 demise during summer is very low over the Lower Amu Darya, as indicated by a median value of
448 zero for June-September, though it is possible since the interdecile range peaks at
449 approximately 1%.

450 To gain a better understanding of the conditions that precede drought onset over the
451 Amu Darya watershed, we explore the likelihood of above and below average 1-m soil
452 moisture, precipitation and 2-m temperature in the CESM simulations as a function of onset
453 month and lead time (Fig. 11). We find that the drought onset precursors in the Upper and
454 Lower Amu Darya regions, and the lead times over which these precursors occur, are similar
455 and vary according to the seasonal cycle. Droughts that begin during October-December are

456 related to high likelihoods of below average precipitation during the onset month and the
457 month prior to onset. This suggests that droughts beginning early in the rainy season may
458 materialize quicker than the other times of the year. Surprisingly, the Upper and Lower regions
459 diverge in terms of 2-m temperatures, as the Upper and Lower regions are related to 40%
460 probabilities of above and below average temperatures, respectively. Droughts the begin
461 during January-April are related to below average precipitation for up to three months prior to
462 drought onset, suggesting that drought onset during the latter part of the rainy season is a
463 comparably slow process. Warm temperatures accompany drought onset over the Upper
464 region during the month of onset and the month prior during January-April while warm
465 temperatures accompany onset over the Lower region during March-May. Drought onset
466 during the warm and dry season, nominally May-October, is related to different conditions than
467 during the cool wet season. Onset during the warm season is related to high probabilities of
468 below average soil moisture in the five months leading up to drought, below average
469 precipitation, and warm temperatures during the month of onset. These conditions suggest
470 that warm season drought onset is not primarily caused by a failure of rains, but rather
471 antecedent soil moisture conditions and warm temperatures.

472 Conditions related to drought demise are less complex than those related to drought
473 onset over the Amu Darya watershed in CESM. Drought demise requires up to just two months
474 of above average precipitation over both regions of the watershed and is not consistently
475 related to above or below average 2-m temperatures (Fig. 12). During the November-April rainy
476 season, drought demise in both regions is related to a greater than 40% probability that
477 precipitation is above average during the month of demise and the month preceding demise.

For the Upper region, there is a slightly elevated probability of below average temperatures during the beginning of the rainy season, but a slightly elevated probability of above average temperatures during the end of the rainy season. For the Lower region, temperatures are not consistently above or below average across the rainy season when drought ends.

While infrequent, drought demise can occur during the May-October dry season (Fig. 10) despite the climatologically meager precipitation that falls during this time of year (Figs. 2-3). Two interesting aspects of dry season drought demise over both Amu Darya regions are a high likelihood that soil moisture remains below average and demise is only related to a 40% probability of above average precipitation during the month of demise (Fig. 12). Drought ends by our definition when soil moisture exceeds the 30th percentile, so it is possible to endure below average soil moisture, defined at less than the 33rd percentile, after drought demise. This is more prominent over the Lower region than the Upper region, but regardless, it calls into question whether a drought can truly end during a dry season.

Since ENSO is a primary driver of rainy season precipitation over the Amu Darya watershed, we explore whether drought phase changes are potentially predictable via knowledge of ENSO state. Indeed, drought phase changes are potentially predictable according to CESM1, as drought onset in the Amu Darya watershed is related to statistically significant increases and decreases in the occurrence of La Niña and El Niño, respectively (Fig. 13). Moreover, the prospects for onset predictability are bolstered by the preferred seasonality in the relationship between drought onset and ENSO occurrence that spans the November-April rainy season over both Upper and Lower regions. In the Upper region, drought onset is related to statistically significant decreases in the occurrence of El Niño during November-April,

consistent with the relationship between El Niño and above average precipitation over the region. By contrast, drought onset over the Upper region is related to statistically significant increases in the occurrence of La Niña during the same extended cold season, which is again consistent with the relationship between La Niña and below average precipitation over the region. Drought onset in the Lower region is similarly related to ENSO, insofar as onset is related to a decreased occurrence of El Niño and an increased occurrence of La Niña during the November-April rainy season.

Drought demise in the Amu Darya watershed is related to a more complicated seasonality of statistically significant changes in the occurrence of El Niño and La Niña (Fig. 14) than drought onset (Fig. 13) in CESM1. Nonetheless, the earth system model simulations suggest that drought demise is potentially predictable via knowledge of the ENSO state; however, the nuances in seasonality must be considered if these relationships are to be applied successfully to prediction. The less regular seasonality in the relationship between drought demise and ENSO occurrence, when compared to onset, is perhaps attributable to the demise and onset time scales. In the earth system model, it takes up to two months of above average precipitation for drought demise (Fig. 12) while it takes up to four months of below average precipitation for drought onset (Fig. 11). Two months of above average precipitation is easier to attain, through processes internal to the atmosphere, than four months of below average precipitation without systematic precipitation forcing from phenomena like ENSO. Further research into the relationship between drought demise and ENSO is needed.

Over the Upper region, drought demise is related to statistically significant increases in the occurrence of El Niño during November and December, no change in the occurrence of El

Niño during January and February, and significant decreases in the occurrence of El Niño during March-June (Fig. 14). Drought demise over the Upper region is related to significant decreases in La Niña during November-February and significant increases in La Niña in August and September, though drought demise during these months is rather unlikely (Fig. 10). Over the Lower region, drought demise is related to increases in the occurrence of El Niño during October-February and decreases in the occurrence of La Niña during November-January and April.

Given the links between decadal variations in Pacific SST (e.g. PDO) and Central and Southwest Asia precipitation (Hoell et al. 2015b; Rana et al. 2019), we conclude the results section with an assessment of whether 10-year spans in which Amu Darya drought is most prevalent are related to an elevated likelihood of below average eastern Pacific SST (Fig. 15). Indeed, CESM1 indicates that decades in which Upper Amu Darya drought is most prevalent are related to a 40-50% likelihood of an SST pattern that is like persistent La Niña-like SST or the cool phase of the PDO (Figs. 15a,b). However, it is important to note that according to CESM1 the most prevalent drought decades are only related to a La Niña-like SST pattern upwards of 50% of the time, thereby suggesting that the majority of prevalent drought periods are related to variability that cannot be explained by persistent SST anomalies. While prevalent Upper Amu Darya drought is related to Pacific SST, the same is not found for the Lower Amu Darya region (Figs. 15c,d).

5. Summary and Discussion

We illustrated characteristics, precursors, and potential predictability of agricultural drought in the Amu Darya watershed that covers the food insecure Central Asia Republics of Afghanistan, Tajikistan, Turkmenistan, and Uzbekistan. Drought, defined by 1-m soil moisture deficits lasting three or more months, was diagnosed in 40 realizations of a fully coupled earth system model spanning 1920-2019 under observed radiative forcing before 2005 and RCP8.5 forcing thereafter. The model realizations were based on the CESM large ensemble version 1, which we found realistically reproduces the variability and seasonal cycles of key hydroclimatic variables estimated by widely used gridded datasets of observed conditions. CESM1 also captures a realistic relationship between Amu Darya weather and climate and ENSO during the region's wintertime rainy season. The 4000 simulated years from CESM1 provides a large sample from which to probe drought behavior than is possible using the existent short and spatially incomplete observed records over Central Asia.

Motivated by the variability of Amu Darya hydroclimate based on traces of 1-m soil moisture in each of the earth system model realizations, we explored characteristics of drought over the region: the prevalence of drought in 100-year periods and the length of individual droughts. In terms of drought prevalence, the Upper and Lower regions demonstrated similarly large possibilities, ranging from just eight years to as many as four decades in drought for every 100 years. In terms of drought length, there is a clear preference for short droughts over the region, as 50% of the droughts in both the Upper and Lower regions persist for less than six and nine months, respectively. However, it must be noted that despite this preference for short droughts, long droughts are a possibility. 5% of droughts last for 2 and 2.75 years over the Upper and Lower regions, respectively, while the longest droughts can last upwards of 8 years.

565 We next explored characteristics of drought onset and demise over the Upper and
566 Lower Amu Darya regions, including seasonality, precursor conditions like precipitation and 2-m
567 temperature, and potential predictability based on ENSO phase. There is a distinct seasonality
568 to drought onset and demise in the Amu Darya watershed. The seasonality of onset and demise
569 does not entirely follow the precipitation seasonal cycle, and consistent with the hydroclimatic
570 variability of the region, the seasonality can vary from one 100-year period to the next. The
571 occurrence of drought onset in the Upper Amu Darya is greatest during November and
572 December, the beginning of the rainy season, and March-May, the end of the rainy season. The
573 occurrence of drought onset in the Lower Amu Darya is similarly high across all months of the
574 November-April rainy season, with a slightly higher occurrence during December than the other
575 months. The occurrence of drought onset during summertime dry season is low for both Upper
576 and Lower regions but is nonetheless possible. The occurrence of drought demise in the Upper
577 Amu Darya is displays a bimodal seasonality, with symmetrical peaks during the beginning of
578 the rainy season (October-December) and the end of the rainy season (March-May). The
579 occurrence of drought demise in the Lower Amu Darya is approximately the same across all
580 months of the rainy season, with a slight peak in November and December. The occurrence of
581 drought demise is low during summertime over both Upper and Lower Amu Darya, given that
582 precipitation during the dry season is generally unable to ameliorate drought.

583 Conditions related to drought onset, and the lead times over which these conditions
584 occur, vary according to the seasonal cycle and are similar for the Upper and Lower Amu Darya
585 regions. Droughts beginning in the early wintertime rainy season, October-December,
586 materialize quicker than other times of the year, as drought onset is related to increased

likelihoods of below average precipitation during the month of onset and the month prior. Droughts beginning during the core of the rainy season, January-April, materialize more slowly, as increased likelihoods of below average precipitation are found up to three months prior to onset. Droughts beginning in the warm and dry season are related to different conditions that during the cool wet season. Onset during this time is not related to failed rains, but rather antecedent soil moisture conditions and warm 2-m temperatures.

Conditions related to drought demise are comparably simple, as demise during the cool wet season is related to just two months of above average precipitation. While infrequent, our definition of drought allows for drought demise during the summertime dry season, and we find that demise during this time of year may not lead to drought recovery. Drought demise during this time of year is related to high likelihoods of below average soil moisture, which sits at the cusp for the threshold of drought demise. A question raised here is whether drought can truly end during a dry season.

Drought onset and demise are potentially predictable via knowledge of the ENSO state, given that drought phase changes are related to statistically significant changes in the occurrence of El Niño and La Niña. However, for knowledge of the ENSO state to be applied successfully to prediction, one must consider the seasonality in the relationships between ENSO and drought phase changes. Drought onset is related to significant changes in ENSO occurrence during the entire November-April rainy season over both Upper and Lower regions, where onset is related to increased (decreased) occurrence of La Niña (El Niño). By contrast, there a complex seasonality to the relationship between drought demise and significant changes in ENSO occurrence. For the Upper region, drought demise is related to significant increases in the

609 occurrence of El Niño during November and December and decreases in the occurrence of El
610 Niño during March-June. For the Lower region, drought demise is related to increases in the
611 occurrence of El Niño during October-February. Given the complex seasonality of the
612 relationships between drought demise and La Niña, the results suggest that onset is more
613 predictable than demise based on ENSO phase.

614 Here we focus on agricultural drought for the practical purpose of building a predictive
615 understanding that may be applied to drought early warning over a region in which rainfed and
616 irrigated agriculture play a vital role in socioeconomic stability and food security. However, our
617 current study does not address other facets of drought, principally hydrological drought, taken
618 here as the availability of water in the Amu Darya river. Amu Darya river flows are critical to
619 water security over the region, as water from the river is used for consumption, irrigating
620 agriculture, and replenishing the diminishing Aral Sea (e.g. Micklin 1988; Micklin 2007). Like
621 analyses of agricultural drought in the Amu Darya watershed, analyses of hydrological drought
622 are lacking, with just a handful of studies having been performed (e.g., Barlow et al. 2008; Apel
623 et al. 2018; Dixon and Wilby 2019). Given that data scarcity over Central Asia in space and time
624 inhibits robust studies of all kinds, it is important that the community creatively and responsibly
625 create new data sources, like Zhou et al. (2018), and appropriately use simulations from models
626 that are deemed fit for purpose to develop a more holistic understanding of drought over the
627 region.

628

629 *Acknowledgements*

We gratefully acknowledge the support of the Famine Early Warning Systems Network, Candida Dewes for discussions about HydroSHEDS, Marty Hoerling for helpful comments and two anonymous reviewers whose suggestions led to a greatly improved manuscript. We also acknowledge the producers and providers of data and simulations used in this analysis. GPCC and UDEL data were accessed from NOAA/OAR/PSL at https://psl.noaa.gov/data/gridded//. GLDAS was accessed from https://disc.gsfc.nasa.gov/datasets?keywords=GLDAS. The CESM1 large ensemble was accessed from http://www.cesm.ucar.edu/projects/community-projects/LENS/data-sets.html. CMIP5 data was accessed from https://esgf-node.llnl.gov/projects/cmip5/. HydroBASINS was accessed from https://www.hydrosheds.org/downloads.

642 **5. References**

643 Apel, H., and Coauthors, 2018: Statistical forecast of seasonal discharge in Central Asia using
644 observational records: development of a generic linear modelling tool for operational
645 water resource management. Hydrol. Earth Syst. Sci., 22, 2225-2254.

646 Barlow, M. A., and M. K. Tippett, 2008: Variability and Predictability of Central Asia River Flows:
647 Antecedent Winter Precipitation and Large-Scale Teleconnections. Journal of
648 Hydrometeorology, 9, 1334-1349.

649 Barlow, M., 2011: The Madden–Julian oscillation influence on Africa and west Asia.
650 Intraseasonal Variability in the Coupled Tropical Ocean-Atmosphere System, W. Lau,
651 and D. Waliser, Eds., Praxis, 477-493.

652 Barlow, M., A. Hoell, and F. Colby, 2007: Examining the wintertime response to tropical
653 convection over the Indian Ocean by modifying convective heating in a full atmospheric
654 model. Geophysical Research Letters, 34, n/a-n/a.

655 Barlow, M., M. Wheeler, B. Lyon, and H. Cullen, 2005: Modulation of Daily Precipitation over
656 Southwest Asia by the Madden–Julian Oscillation. Monthly Weather Review, 133, 3579-
657 3594.

658 Bearak, B., 2000-06-08: In Crippled Afghanistan, a Torturing Drought. New York Times, A00012

659 Capotondi, A., and Coauthors, 2014: Understanding ENSO Diversity. Bulletin of the American
660 Meteorological Society, 96, 921-938.

661 British Broadcasting Company, cited 2019: Afghan drought displacing more people than Taliban
662 conflict. [Available online at https://www.bbc.com/news/world-asia-45872897.]

663 Dixon, S. G., and R. L. Wilby, 2019: A seasonal forecasting procedure for reservoir inflows in
664 Central Asia. River Research and Applications, 0.

665 Gall, C., 2008-09-18: Cornered by War and Drought, Afghans Fear Hungry Winter. New York
666 Times, A1.

667 Gerlitz, L., E. Steirou, C. Schneider, V. Moron, S. Vorogushyn, and B. Merz, 2018: Variability of
668 the Cold Season Climate in Central Asia. Part I: Weather Types and Their Tropical and
669 Extratropical Drivers. Journal of Climate, 31, 7185-7207.

670 Gerlitz, L., E. Steirou, C. Schneider, V. Moron, S. Vorogushyn, and B. Merz, 2019: Variability of
671 the Cold Season Climate in Central Asia. Part II: Hydroclimatic Predictability. Journal of
672 Climate, 32, 6015-6033.

673 Gill, A. E., 1980: Some simple solutions for heat-induced tropical circulation. Quarterly Journal
674 of the Royal Meteorological Society, 106, 447-462.

675 Hoell, A., M. Barlow, and R. Saini, 2012: The Leading Pattern of Intraseasonal and Interannual
676 Indian Ocean Precipitation Variability and Its Relationship with Asian Circulation during
677 the Boreal Cold Season. Journal of Climate, 25, 7509-7526.

678 Hoell, A., and C. Funk, 2013: The ENSO-Related West Pacific Sea Surface Temperature Gradient.
679 Journal of Climate, 26, 9545-9562.

680 Hoell, A., M. Barlow, and R. Saini, 2013: Intraseasonal and Seasonal-to-Interannual Indian
681 Ocean Convection and Hemispheric Teleconnections. Journal of Climate, 26, 8850-8867.

682 Hoell, A., C. Funk, and M. Barlow, 2014a: The regional forcing of Northern hemisphere drought
683 during recent warm tropical west Pacific Ocean La Niña events. Clim Dyn, 42, 3289-3311.

684 Hoell, A., C. Funk, and M. Barlow, 2014b: La Niña diversity and Northwest Indian Ocean Rim
685 teleconnections. Clim Dyn, 43, 2707-2724.

686 Hoell, A., S. Shukla, M. Barlow, F. Cannon, C. Kelley, and C. Funk, 2015a: The Forcing of Monthly
687 Precipitation Variability over Southwest Asia during the Boreal Cold Season. Journal of
688 Climate, 28, 7038-7056.

689 Hoell, A., C. Funk, and M. Barlow, 2015b: The Forcing of Southwestern Asia Teleconnections by
690 Low-Frequency Sea Surface Temperature Variability during Boreal Winter. *J.*
691 *Climate,* **28**, 1511–1526, https://doi.org/10.1175/JCLI-D-14-00344.1

692 Hoell, A., M. Barlow, F. Cannon, and T. Xu, 2017a: Oceanic Origins of Historical Southwest Asia
693 Precipitation During the Boreal Cold Season. Journal of Climate, 30, 2885-2903.

694 Hoell, A., C. Funk, M. Barlow, and F. Cannon, 2017b: A Physical Model for Extreme Drought over
695 Southwest Asia. Climate Extremes, John Wiley & Sons, Inc., 283-298.

696 Hoell, A., F. Cannon, and M. Barlow, 2018a: Middle East and Southwest Asia Daily Precipitation
697 Characteristics Associated with the Madden–Julian Oscillation during Boreal Winter.
698 Journal of Climate, 31, 8843-8860.

699 Hoell, A., M. Barlow, T. Xu, and T. Zhang, 2018b: Cold Season Southwest Asia Precipitation
700 Sensitivity to El Niño–Southern Oscillation Events. Journal of Climate, 31, 4463-4482.

701 Huang, B., and Coauthors, 2017: Extended Reconstructed Sea Surface Temperature, Version 5
702 (ERSSTv5): Upgrades, Validations, and Intercomparisons. Journal of Climate, 30, 8179-8205.

703 Hunke, E. C., D. A. Hebert, and O. Lecomte, 2013: Level-ice melt ponds in the Los Alamos sea ice
704 model, CICE. Ocean Modelling, 71, 26-42.

705 Hurrell, J. W., J. J. Hack, D. Shea, J. M. Caron, and J. Rosinski, 2008: A New Sea Surface
706 Temperature and Sea Ice Boundary Dataset for the Community Atmosphere Model.
707 Journal of Climate, 21, 5145-5153.

708 Al Jazeera, cited 2019: Water shortages worsen in Afghanistan as drought persists. [Available
709 online at https://www.aljazeera.com/news/2018/12/water-shortages-worsen-
710 afghanistan-drought-persists-181223111821371.html.]

711 Johnson, N. C., 2013: How Many ENSO Flavors Can We Distinguish?*. Journal of Climate, 26,
712 4816-4827.

713 Kay, J. E., and Coauthors, 2015: The Community Earth System Model (CESM) Large Ensemble
714 Project: A Community Resource for Studying Climate Change in the Presence of Internal
715 Climate Variability. Bulletin of the American Meteorological Society, 96, 1333-1349.

716 Keyantash, J., and J. A. Dracup, 2002: The Quantification of Drought: An Evaluation of Drought
717 Indices. Bulletin of the American Meteorological Society, 83, 1167-1180.

718 Krishnamurti, T. N., 1961: THE SUBTROPICAL JET STREAM OF WINTER. Journal of Meteorology,
719 18, 172-191.

720 Lamarque, J.-F., and Coauthors, 2011: Global and regional evolution of short-lived radiatively-
721 active gases and aerosols in the Representative Concentration Pathways. Climatic
722 Change, 109, 191.

723 Lamarque, J. F., and Coauthors, 2010: Historical (1850–2000) gridded anthropogenic and
724 biomass burning emissions of reactive gases and aerosols: methodology and application.
725 Atmos. Chem. Phys., 10, 7017-7039.

726 Lawrence, D. M., and Coauthors, 2011: Parameterization improvements and functional and
727 structural advances in Version 4 of the Community Land Model. Journal of Advances in
728 Modeling Earth Systems, 3.

729 Lehner, B., and G. Grill, 2013: Global river hydrography and network routing: baseline data and
730 new approaches to study the world's large river systems. Hydrological Processes, 27,
731 2171-2186.

732 Lehner, B., K. Verdin, and A. Jarvis, 2008: New Global Hydrography Derived From Spaceborne
733 Elevation Data. Eos, Transactions American Geophysical Union, 89, 93-94.

734 Madden, R. A., and P. R. Julian, 1972: Description of Global-Scale Circulation Cells in the Tropics
735 with a 40–50 Day Period. Journal of the Atmospheric Sciences, 29, 1109-1123.

736 Madden, R. A., and P. R. Julian, 1994: Observations of the 40–50-Day Tropical Oscillation—A
737 Review. Monthly Weather Review, 122, 814-837.

738 Mantua, N. J., S. R. Hare, Y. Zhang, J. M. Wallace, and R. C. Francis, 1997: A Pacific Interdecadal
739 Climate Oscillation with Impacts on Salmon Production. Bulletin of the American
740 Meteorological Society, 78, 1069-1079.

741 Martyn, D., 1992: Climates of the World. Elsevier, 436 pp.

742 Matsuno, T., 1966: Quasi-Geostrophic Motions in the Equatorial Area. Journal of the
743 Meteorological Society of Japan. Ser. II, 44, 25-43.

744 Meinshausen, M., and Coauthors, 2011: The RCP greenhouse gas concentrations and their
745 extensions from 1765 to 2300. Climatic Change, 109, 213.

746 Menne, M. J., C. N. Williams, B. E. Gleason, J. J. Rennie, and J. H. Lawrimore, 2018: The Global
747 Historical Climatology Network Monthly Temperature Dataset, Version 4. Journal of
748 Climate, 31, 9835-9854.

749 Micklin, P. P., 1988: Desiccation of the Aral Sea: A Water Management Disaster in the Soviet
750 Union. Science, 241, 1170.

751 Micklin, P., 2007: The Aral Sea Disaster. Annual Review of Earth and Planetary Sciences, 35, 47-
752 72.

753 Mirzabaev, A., 2018: Improving the Resilience of Central Asian Agriculture to Weather
754 Variability and Climate Change. Climate Smart Agriculture : Building Resilience to
755 Climate Change, L. Lipper, N. McCarthy, D. Zilberman, S. Asfaw, and G. Branca, Eds.,
756 Springer International Publishing, 477-495.

Mo, K. C., 2011: Drought onset and recovery over the United States. Journal of Geophysical Research: Atmospheres, 116.

Food and Agricultural Organization of the United Nations (FAO), cited 2019: The State of Food Security and Nutrition in Europe and Central Asia, FAO, 68 pp. [Available online at http://www.fao.org/3/a-i8194e.pdf.]

FEWS NET, cited 2019: Drought, Conflict, and Displacement drive food insecurity across the country. [Available online at http://fews.net/central-asia/afghanistan/food-security-outlook-update/august-2018.]

Newman, M., and Coauthors, 2016: The Pacific Decadal Oscillation, Revisited. Journal of Climate.

Shahriar Pervez, M., M. Budde, and J. Rowland, 2014: Mapping irrigated areas in Afghanistan over the past decade using MODIS NDVI. Remote Sensing of Environment, 149, 155-165.

World Meteorological Organization, 1975: Drought and Agriculture, WMO Technical Document 392, 127 pp.

World Bank, cited 2019: Data Bank: World Bank Development Indicators. [Available online at https://databank.worldbank.org/reports.aspx?source=2&series=NV.AGR.TOTL.ZS&country=AFG,TJK,UZB,TKM.]

World Bank, cited 2019: GNI Per Capita, Atlas Method. [Available online at https://data.worldbank.org/indicator/ny.gnp.pcap.cd.]

776 Rakhmatullaev, S., and Coauthors, 2009: Groundwater resources use and management in the
777 Amu Darya River Basin (Central Asia). Environmental Earth Sciences, 59, 1183.

778 Rana, S., J. McGregor, and J. Renwick, 2017: Wintertime precipitation climatology and ENSO
779 sensitivity over central southwest Asia. International Journal of Climatology, 37, 1494-
780 1509.

781 Rana, S., J. McGregor, and J. Renwick, 2019: Dominant modes of winter precipitation variability
782 over Central Southwest Asia and inter-decadal change in the ENSO teleconnection. Clim
783 Dyn.

784 Rana, S., J. Renwick, J. McGregor, and A. Singh, 2017: Seasonal Prediction of Winter
785 Precipitation Anomalies over Central Southwest Asia: A Canonical Correlation Analysis
786 Approach. Journal of Climate, 31, 727-741.

787 Rodell, M., and Coauthors, 2004: The Global Land Data Assimilation System. Bulletin of the
788 American Meteorological Society, 85, 381-394.

789 Schneider, U., A. Becker, P. Finger, A. Meyer-Christoffer, M. Ziese, and B. Rudolf, 2014: GPCC's
790 new land surface precipitation climatology based on quality-controlled in situ data and
791 its role in quantifying the global water cycle. Theor Appl Climatol, 115, 15-40.

792 U.S. Department of Agriculture Foreign Agricultural Service: AFGHANISTAN: Severe Drought
793 Causes Major Decline in 2008/09 Wheat Production. [Available online at
794 https://ipad.fas.usda.gov/highlights/2008/08/Afghanistan%20Drought/.]

795 Smith, R., and Coauthors, 2010: The Parallel Ocean Program (POP) Reference Manual: Ocean
796 Component of the Community Climate System Model (CCSM) and Community Earth
797 System Model (CESM), 127 pp.

798 Svoboda, M., and Coauthors, 2002: THE DROUGHT MONITOR. Bulletin of the American
799 Meteorological Society, 83, 1181-1190.

800 Taylor, K. E., R. J. Stouffer, and G. A. Meehl, 2011: An Overview of CMIP5 and the Experiment
801 Design. Bulletin of the American Meteorological Society, 93, 485-498.

802 Tebaldi, C., J. M. Arblaster, and R. Knutti, 2011: Mapping model agreement on future climate
803 projections. Geophysical Research Letters, 38.

804 Willmott, C. J., and K. Matsuura: Terrestrial Air Temperature and Precipitation: Monthly and
805 Annual Time Series (1950 - 1999). [Available online at
806 http://climate.geog.udel.edu/~climate/html_pages/download.html.]

807 Zhang, C., 2005: Madden-Julian Oscillation. Reviews of Geophysics, 43.

808 Zhang, Y., J. M. Wallace, and D. S. Battisti, 1997: ENSO-like Interdecadal Variability: 1900–93.
809 Journal of Climate, 10, 1004-1020.

810 Zhou, H., E. Aizen, and V. Aizen, 2018: Constructing a long-term monthly climate data set in
811 central Asia. International Journal of Climatology, 38, 1463-1475.

812

Table Captions

Table 1: The 37 CMIP5 models considered.

817 Table 1: The 37 CMIP5 models considered.

Model	Institution
INM-CM4	Institute for Numerical Mathematics
BCC-CSM1.1	Beijing Climate Center
BCC-CSM1.1(m)	Beijing Climate Center
NorESM1-M	Norwegian Climate Centre
NorESM1-ME	Norwegian Climate Centre
MRI-CGCM3	Meteorological Research Institute
MPI-ESM-LR	Max Planck Institute for Meteorology
MPI-ESM-MR	Max Planck Institute for Meteorology
MPI-ESM-P	Max Planck Institute for Meteorology
MIROC5	Atmosphere and Ocean Research Institute (The University of Tokyo), National Institute for Environmental Studies, and Japan Agency for Marine-Earth Science and Technology
MIROC-ESM	Atmosphere and Ocean Research Institute (The University of Tokyo), National Institute for Environmental Studies, and Japan Agency for Marine-Earth Science and Technology
MIROC-ESM-CHEM	Atmosphere and Ocean Research Institute (The University of Tokyo), National Institute for Environmental Studies, and Japan Agency for Marine-Earth Science and Technology
IPSL-CM5A-LR	Institut Pierre-Simon Laplace
IPSL-CM5A-MR	Institut Pierre-Simon Laplace
IPSL-CM5B-LR	Institut Pierre-Simon Laplace
HadGEM2-A	Met Office Hadley Centre
HadGEM2-CC	Met Office Hadley Centre
HadGEM2-ES	Met Office Hadley Centre
GISS-E2-H	NASA Goddard Institute for Space Studies
GISS-E2-R	NASA Goddard Institute for Space Studies
GFDL-CM3	Geophysical Fluid Dynamics Laboratory
GFDL-ESM2G	Geophysical Fluid Dynamics Laboratory
GFDL-ESM2M	Geophysical Fluid Dynamics Laboratory
FIO-ESM	The First Institute of Oceanography, SOA, China
FGOALS-g2	LASG, Institute of Atmospheric Physics, Chinese Academy of Sciences; and CESS, Tsinghua University
FGOALS-s2	LASG, Institute of Atmospheric Physics, Chinese Academy of Sciences
CanESM2	Canadian Centre for Climate Modelling and Analysis
CSIRO-Mk3.6.0	Commonwealth Scientific and Industrial Research Organisation in collaboration with the Queensland Climate Change Centre of Excellence
CNRM-CM5	Centre National de Recherches Meteorologiques / Centre Europeen de Recherche et Formation Avancees en Calcul Scientifique

CMCC-CM	Centro Euro-Mediterraneo per I Cambiamenti Climatici
CMCC-CMS	Centro Euro-Mediterraneo per I Cambiamenti Climatici
CESM1(CAM5)	National Science Foundation, Department of Energy, National Center for Atmospheric Research
CESM1(BGC)	National Science Foundation, Department of Energy, National Center for Atmospheric Research
CCSM4	National Center for Atmospheric Research
BNU-ESM	College of Global Change and Earth System Science, Beijing Normal University
ACCESS1.0	CSIRO (Commonwealth Scientific and Industrial Research Organisation, Australia), and BOM (Bureau of Meteorology, Australia)
ACCESS1.3	CSIRO (Commonwealth Scientific and Industrial Research Organisation, Australia), and BOM (Bureau of Meteorology, Australia)

818

819

820

821 **Figure Captions**

822 Figure 1: (a) The four countries in pink – Tajikistan, Afghanistan, Uzbekistan and Turkmenistan –
823 that contain most of the land area in the Amu Darya watershed. (b) Elevation above
824 mean sea level (km) and representation of the Amu Darya watershed. The perimeter of
825 the heavy polygon is the HydroBASINS Level 3 representation of the Amu Darya
826 watershed while the light polygons are the HydroBASINS Level 4 representation of the
827 sub-basins that make up the Amu Darya. The heavy pink and blue polygons represent
828 the Upper and Lower Amu Darya regions, respectively.

829 Figure 2: (a) Average count of stations reporting per grid point in the GPCC precipitation dataset
830 for 1920-2016 in the Upper (pink) and Lower (orange) Amu Darya regions. Number of
831 stations reporting in the GPCC precipitation dataset in (b) January 1950 and (c) January
832 1980.

833 Figure 3: 1920-2019 monthly average precipitation for a single realization of 37 CMIP5 models
834 shown in Table 1 (gray), 40 CESM realizations (light pink), the average of the 40 CESM
835 realizations (dark pink) and GPCC (blue) for the (a) Upper and (b) Lower Amu Darya
836 regions. CMIP5 models are not individually identified for clarity.

837 Figure 4: Boxplots of monthly (top row) precipitation, (center row) 2-m air temperature and
838 (bottom row) 1-m soil moisture for the (left column) Upper and (right column) Lower
839 Amu Darya regions in 40 CESM realizations (pink) and observed estimates (orange).
840 Precipitation and 2-m temperature are based on data from 1920-2019 and 1-m soil
841 moisture draws on data from 1979-2018. For the boxplots, whiskers denote the

842 interdecile range, the boxes the interquartile range, and the horizonal line inside the
843 box the median.

844 Figure 5: Annual average precipitation (mm) for (a) GPCC and (b) CESM. The pink and orange
845 polygons represent the Upper and Lower Amu Darya regions, respectively.

846 Figure 6: For the (a) Upper and (b) Lower Amu Darya regions, 30-year end point correlations
847 between precipitation and the Niño3.4 index. Plotted are the observed estimate based
848 on GPCC (pink line), 40 CESM realizations (gray lines) and the CESM realization (orange)
849 that is most like the observed estimate, the correlation with the lowest root mean
850 square difference from the observed estimate since 1970.

851 Figure 7: Time series of 1-m soil moisture percentiles in the Lower Amu Darya region from the
852 second ensemble member of CESM, as an illustration of the drought definition. Drought
853 begins in March 1982 and ends in December 1983.

854 Figure 8: Time series of Lower Amu Darya 1-m soil moisture percentiles from the CESM
855 simulations. All 40 ensemble members are shown in gray, ensemble member 37
856 (wettest) is shown in pink, ensemble member 39 (driest) is shown in orange and the
857 ensemble average is shown in black.

858 Figure 9: Box plots of (a) drought prevalence in years and (b) drought length in years based on
859 the 40 CESM realizations in the Upper and Lower Amu Darya regions.

860 Figure 10: Monthly occurrence of drought (left column) onset and (right column) demise in the
861 (top row) Upper and (bottom row) Lower Amu Darya regions. The bars represent the

862 median occurrence and the whiskers the interdecile range. The median and the deciles
863 are obtained from the drought occurrence across each of the 40 100-year CESM
864 realizations.

865 Figure 11: The probability of above or below average (left column) 1-m soil moisture, (center
866 column) precipitation and (right column) 2-m air temperature for the (top row) Upper
867 and (bottom row) Lower Amu Darya regions related to drought onset in the CESM
868 realizations. 0 months prior indicates the month of drought onset and 5 months prior
869 indicates five months prior to drought onset. The most likely category is plotted when it
870 exceeds 40%.

871 Figure 12: The probability of above or below average (left column) 1-m soil moisture, (center
872 column) precipitation and (right column) 2-m air temperature for the (top row) Upper
873 and (bottom row) Lower Amu Darya regions related to drought demise in the CESM
874 realizations. 0 months prior indicates the month of drought demise and 5 months prior
875 indicates five months prior to drought demise. The most likely category is plotted when
876 it exceeds 40%.

877 Figure 13: Occurrence of El Niño (left column) and (right column) La Niña in the (top row) Upper
878 and (bottom row) Lower Amu Darya regions related to drought onset in the CESM
879 realizations. Red (blue) bars indicate statistically significant increases (decreases) in
880 occurrence at $p<0.05$ based on resampling. The gray shading indicates the range of
881 values at $p>0.05$. El Niño and La Niña occur when the Niño3.4 index exceeds 0.5°C and -

882 0.5°C, respectively. The Niño3.4 index is defined as the area averaged SST anomaly over
883 the region 5°S-5°N, 170°W-120°W.

884 Figure 14: Occurrence of El Niño (left column) and (right column) La Niña in the (top row) Upper
885 and (bottom row) Lower Amu Darya regions related to drought demise in the CESM
886 realizations. Red (blue) bars indicate statistically significant increases (decreases) in
887 occurrence at $p<0.05$ based on resampling. The gray shading indicates the range of
888 values at $p>0.05$. El Niño and La Niña occur when the Niño3.4 index exceeds 0.5°C and -
889 0.5°C, respectively. The Niño3.4 index is defined as the area averaged SST anomaly over
890 the region 5°S-5°N, 170°W-120°W.

891 Figure 15: The probability of above or below average (left column) 1-m soil moisture and (right
892 column) SST for the (top row) Upper and (bottom row) Lower Amu Darya regions during
893 10-year periods in which drought was most prevalent in the CESM realizations. The most
894 likely category is plotted when it exceeds 40%. Most prevalent drought decades are
895 defined as the top decile of drought occurrence in non-overlapping 120-month periods.

896

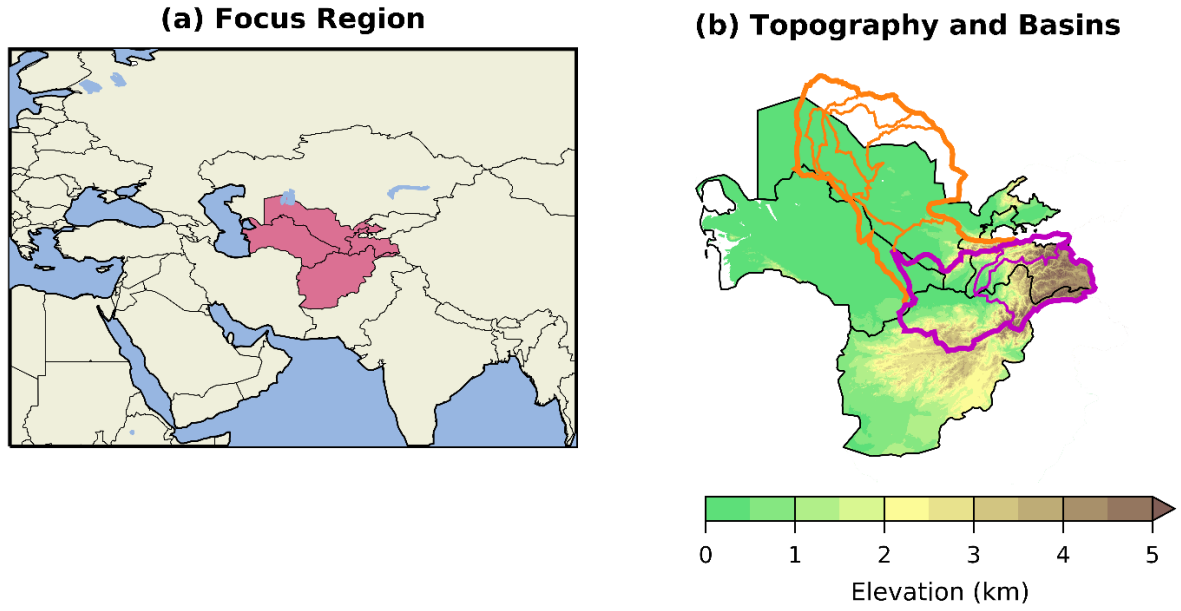

Figure 1: (a) The four countries in pink – Tajikistan , Afghanistan , Uzbekistan and Turkmenistan – that contain most of the land area in the Amu Darya watershed. (b) Elevation above mean sea level (km) and representation of the Amu Darya watershed. The perimeter of the heavy polygon is the HydroBASINS Level 3 representation of the Amu Darya watershed while the light polygons are the HydroBASINS Level 4 representation of the sub-basins that make up the Amu Darya. The heavy pink and blue polygons represent the Upper and Lower Amu Darya regions, respectively.

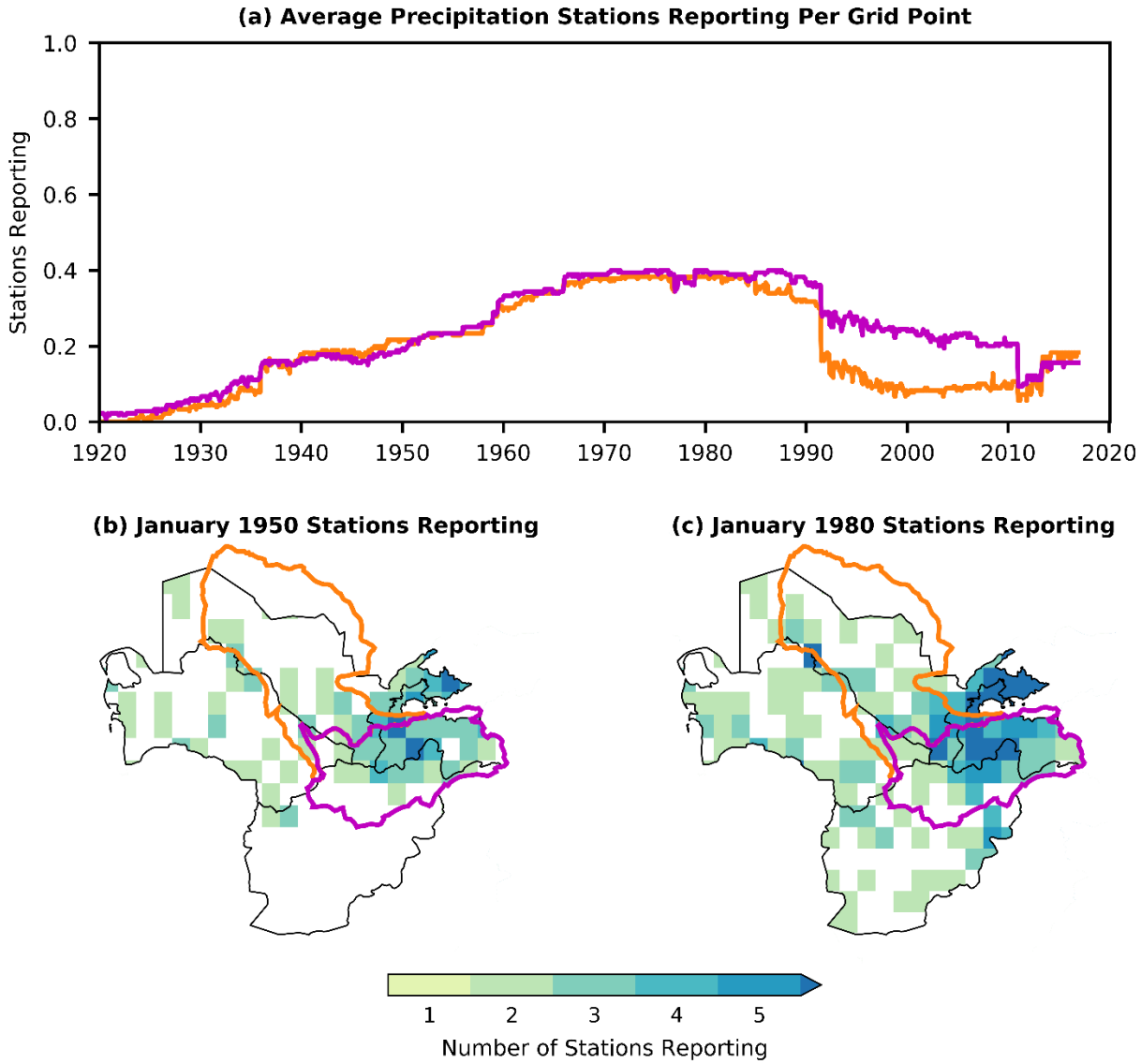

Figure 2: (a) Average count of stations reporting per grid point in the GPCC precipitation dataset for 1920-2016 in the Upper (pink) and Lower (orange) Amu Darya regions. Number of stations reporting in the GPCC precipitation dataset in (b) January 1950 and (c) January 1980.

907

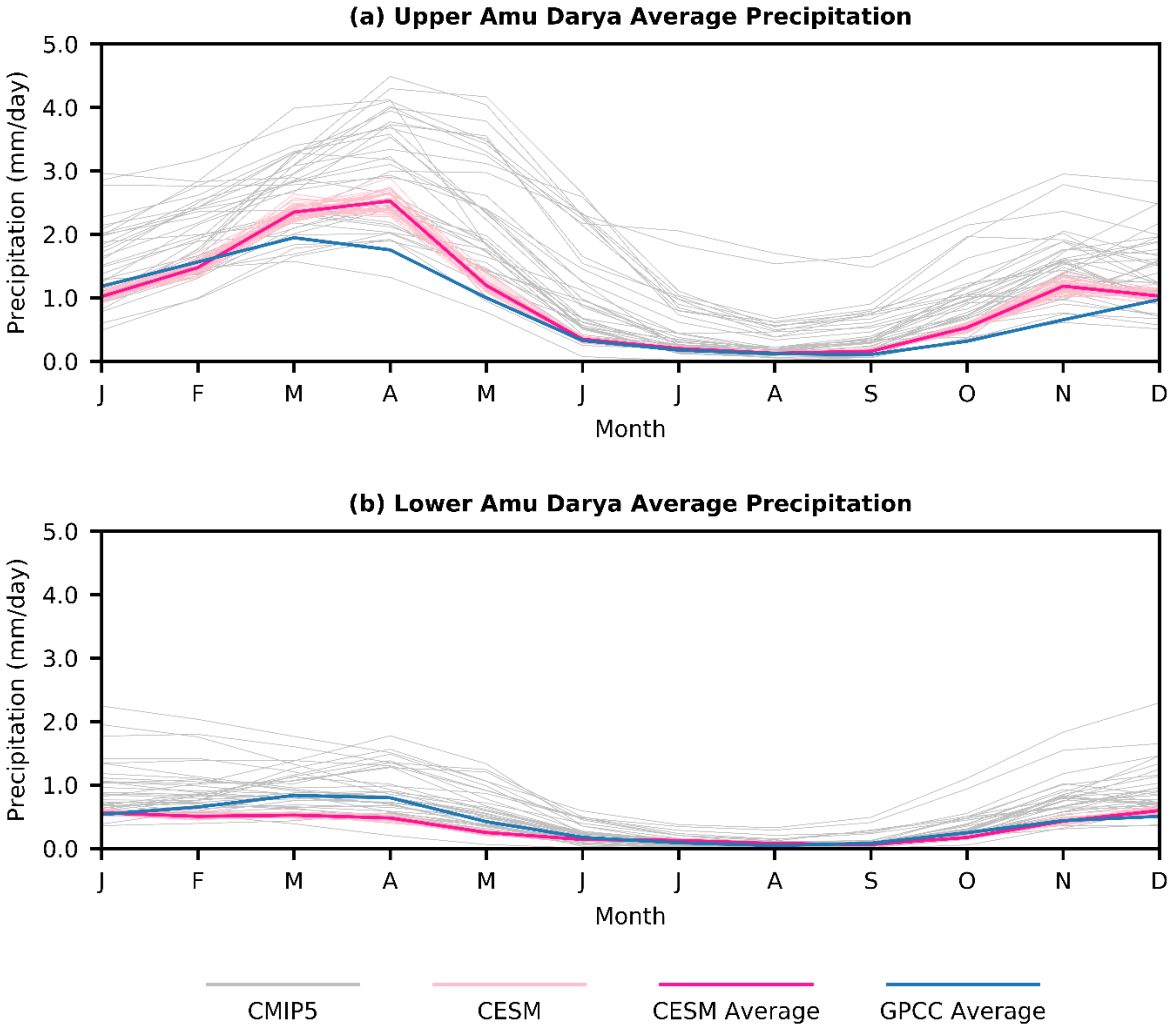

Figure 3: 1920-2019 monthly average precipitation for a single realization of 37 CMIP5 models shown in Table 1 (gray), 40 CESM realizations (light pink), the average of the 40 CESM realizations (dark pink) and GPCC (blue) for the (a) Upper and (b) Lower Amu Darya regions. CMIP5 models are not individually identified for clarity.

908

909

910

911

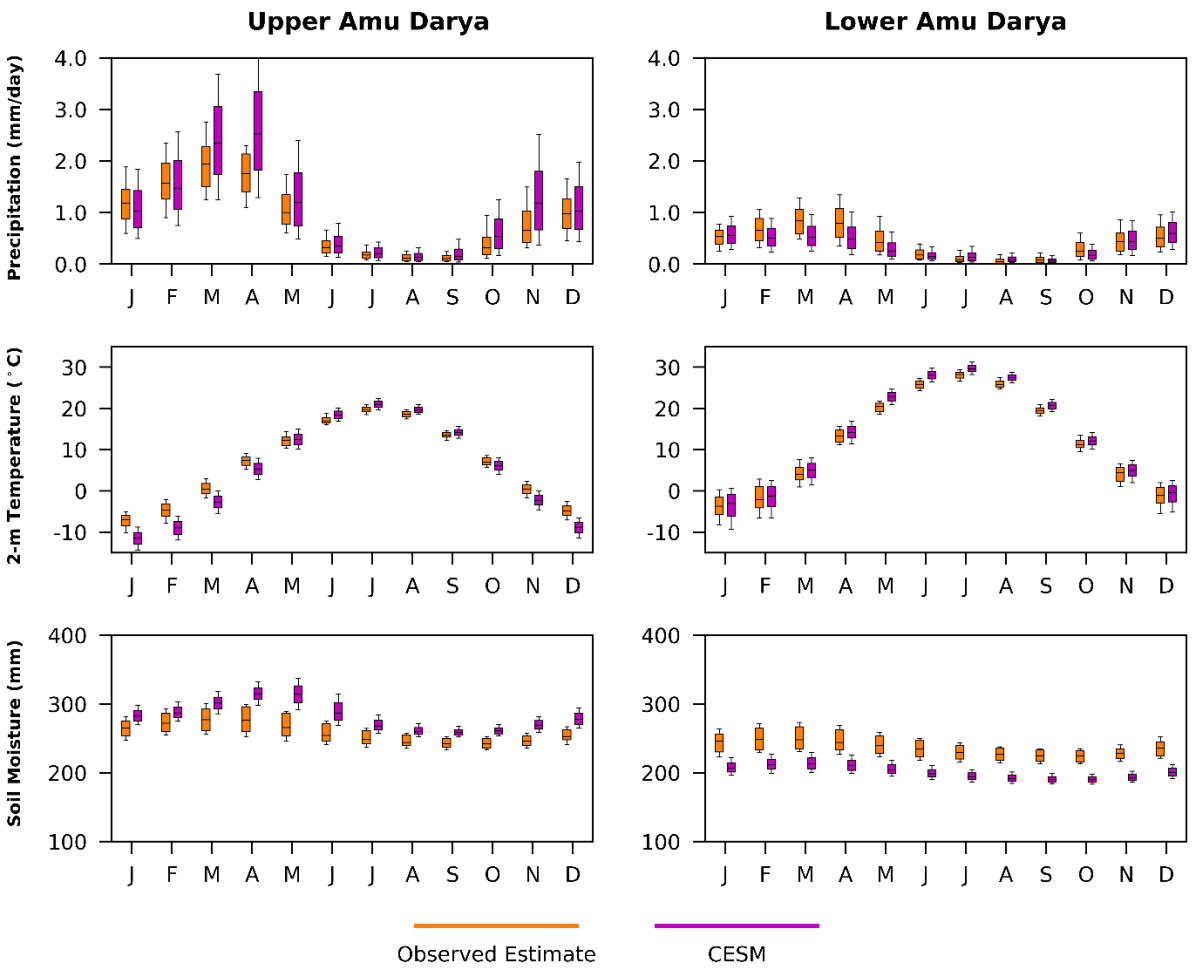

Figure 4: Boxplots of monthly (top row) precipitation, (center row) 2-m air temperature and (bottom row) 1-m soil moisture for the (left column) Upper and (right column) Lower Amu Darya regions in 40 CESM realizations (pink) and observed estimates (orange). Precipitation and 2-m temperature are based on data from 1920-2019 and 1-m soil moisture draws on data from 1979-2018. For the boxplots, whiskers denote the interdecile range, the boxes the interquartile range, and the horizonal line inside the box the median.

912

913

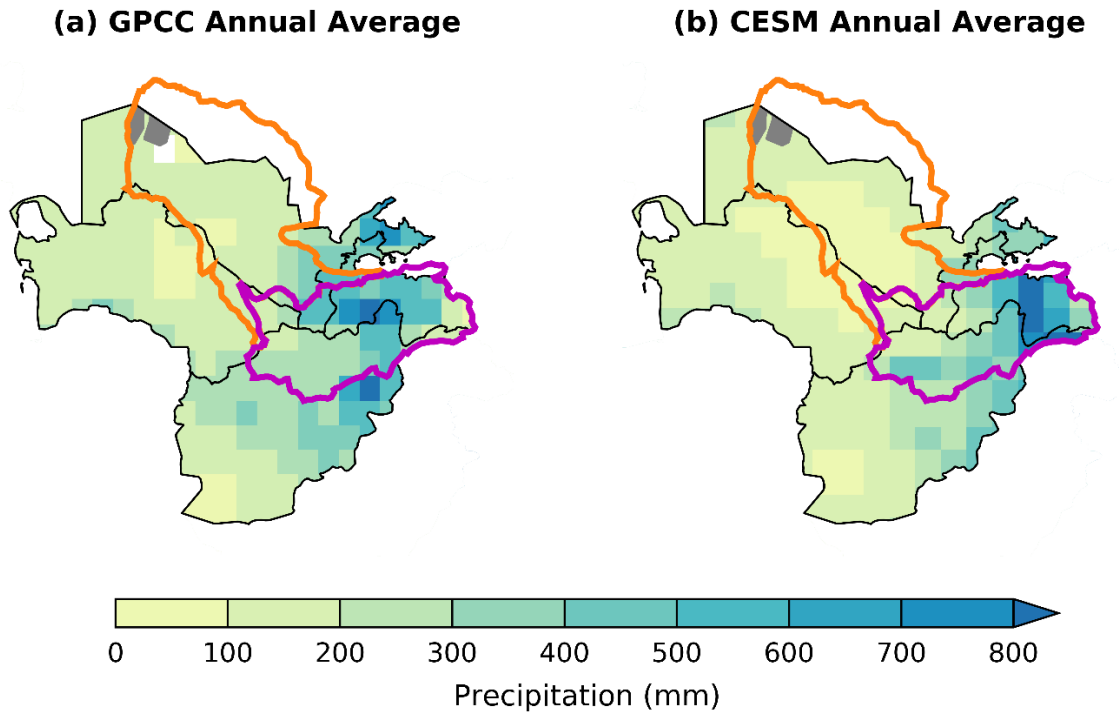

Figure 5: Annual average precipitation (mm) for (a) GPCC and (b) CESM. The pink and orange polygons represent the Upper and Lower Amu Darya regions, respectively.

914

915

916

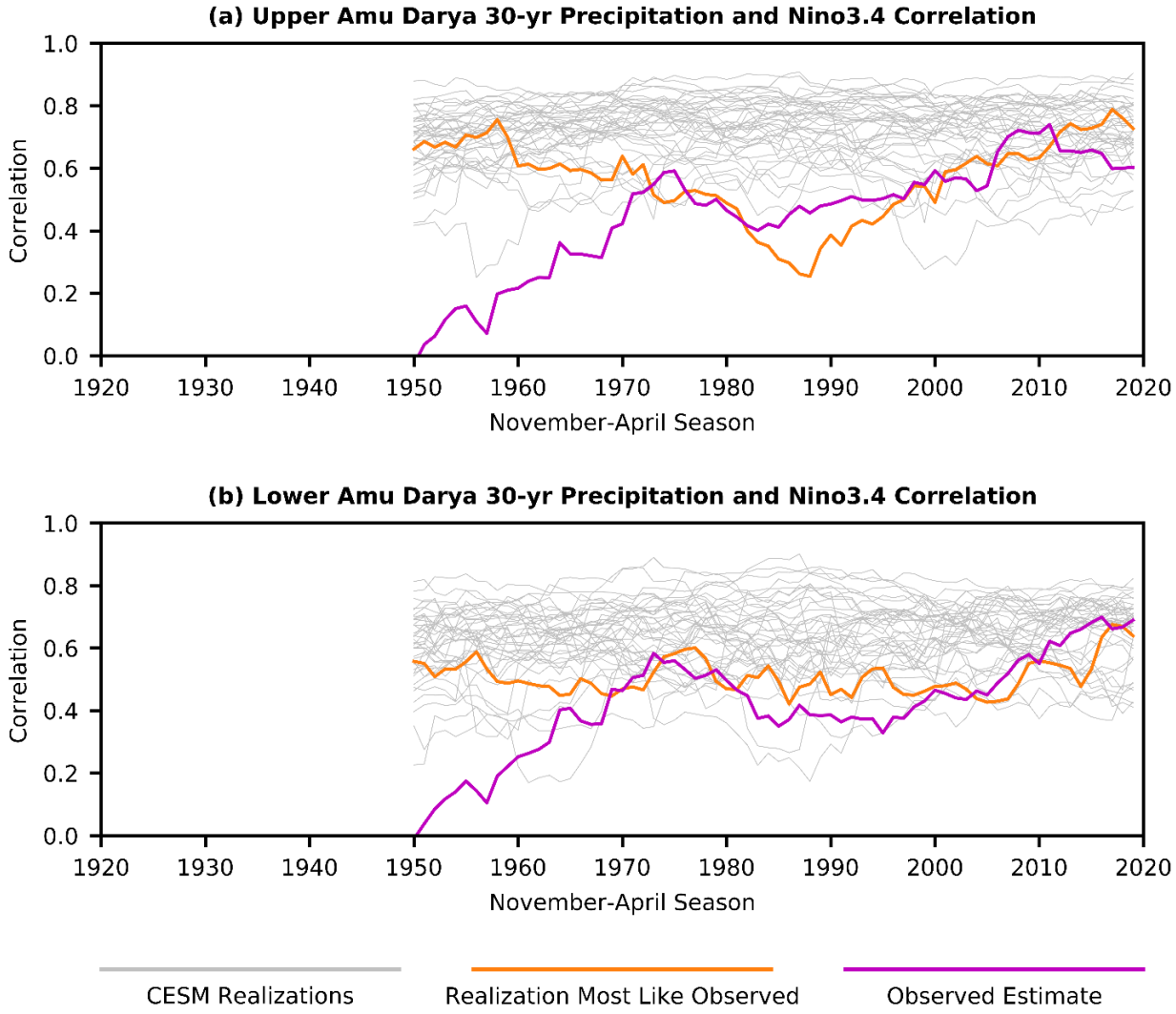

Figure 6: For the (a) Upper and (b) Lower Amu Darya regions, 30-year end point correlations between precipitation and the Niño3.4 index. Plotted are the observed estimate based on GPCC (pink line), 40 CESM realizations (gray lines) and the CESM realization (orange) that is most like the observed estimate, the correlation with the lowest root mean square difference from the observed estimate since 1970.

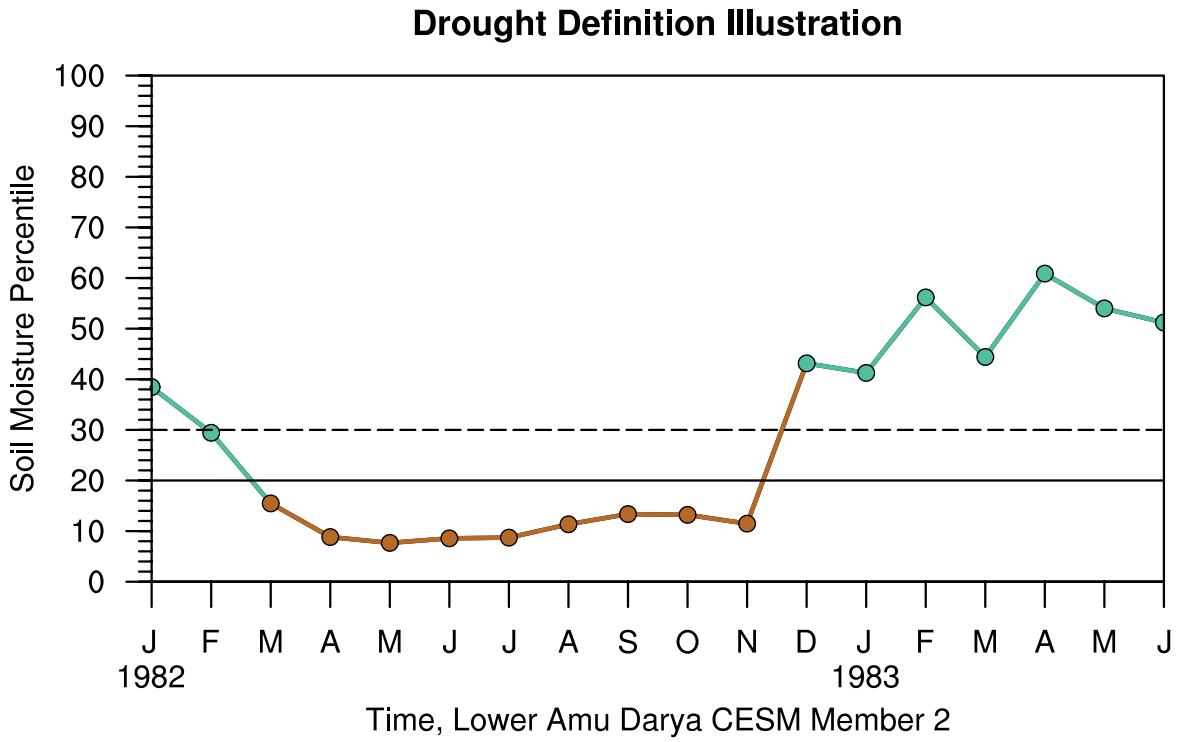

Figure 7: Time series of 1-m soil moisture percentiles in the Lower Amu Darya region from the second ensemble member of CESM, as an illustration of the drought definition. Drought begins in March 1982 and ends in December 1983.

926

927

928

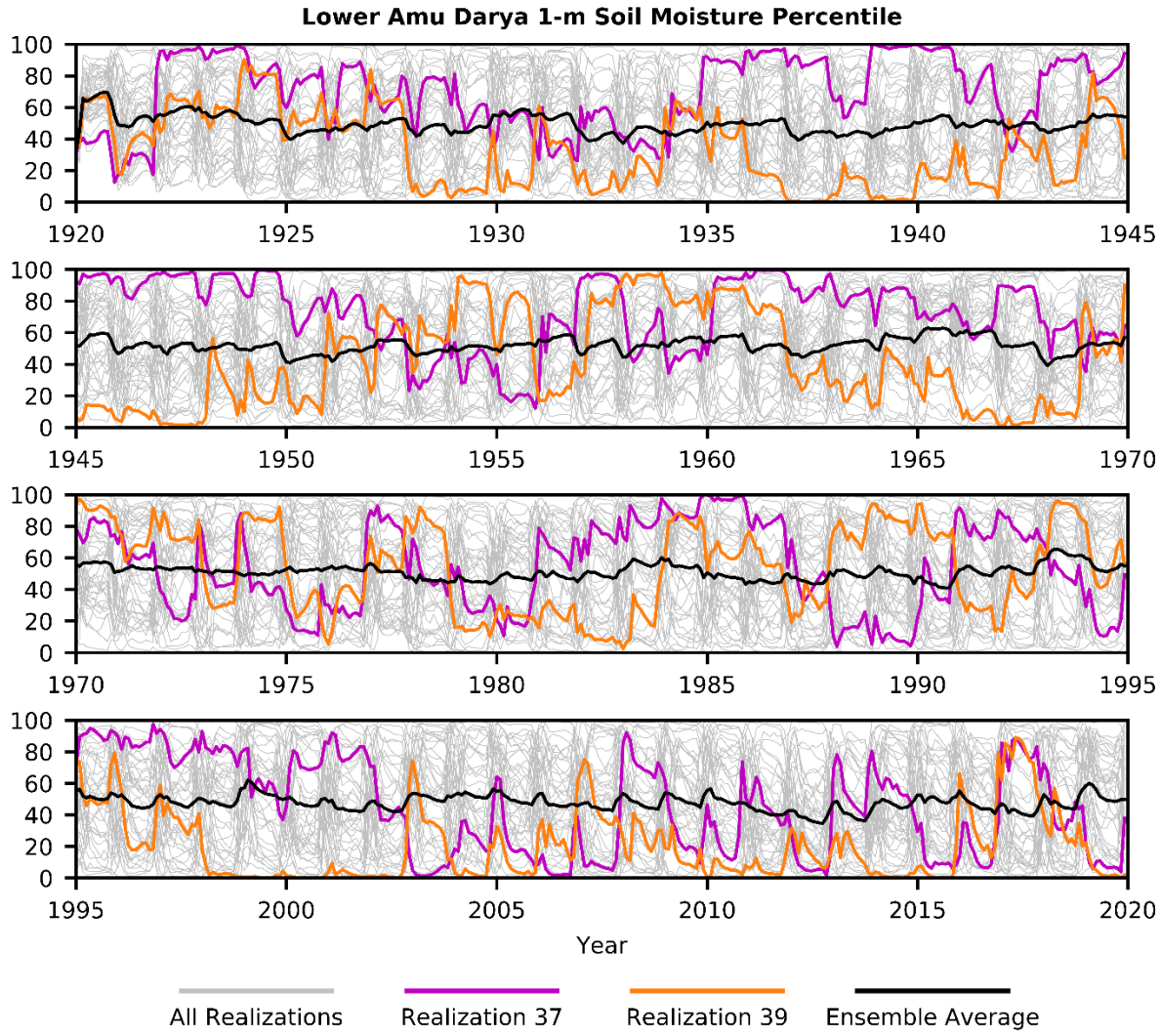

Figure 8: Time series of Lower Amu Darya 1-m soil moisture percentiles from the CESM simulations. All 40 ensemble members are shown in gray, ensemble member 37 (wettest) is shown in pink, ensemble member 39 (driest) is shown in orange and the ensemble average is shown in black.

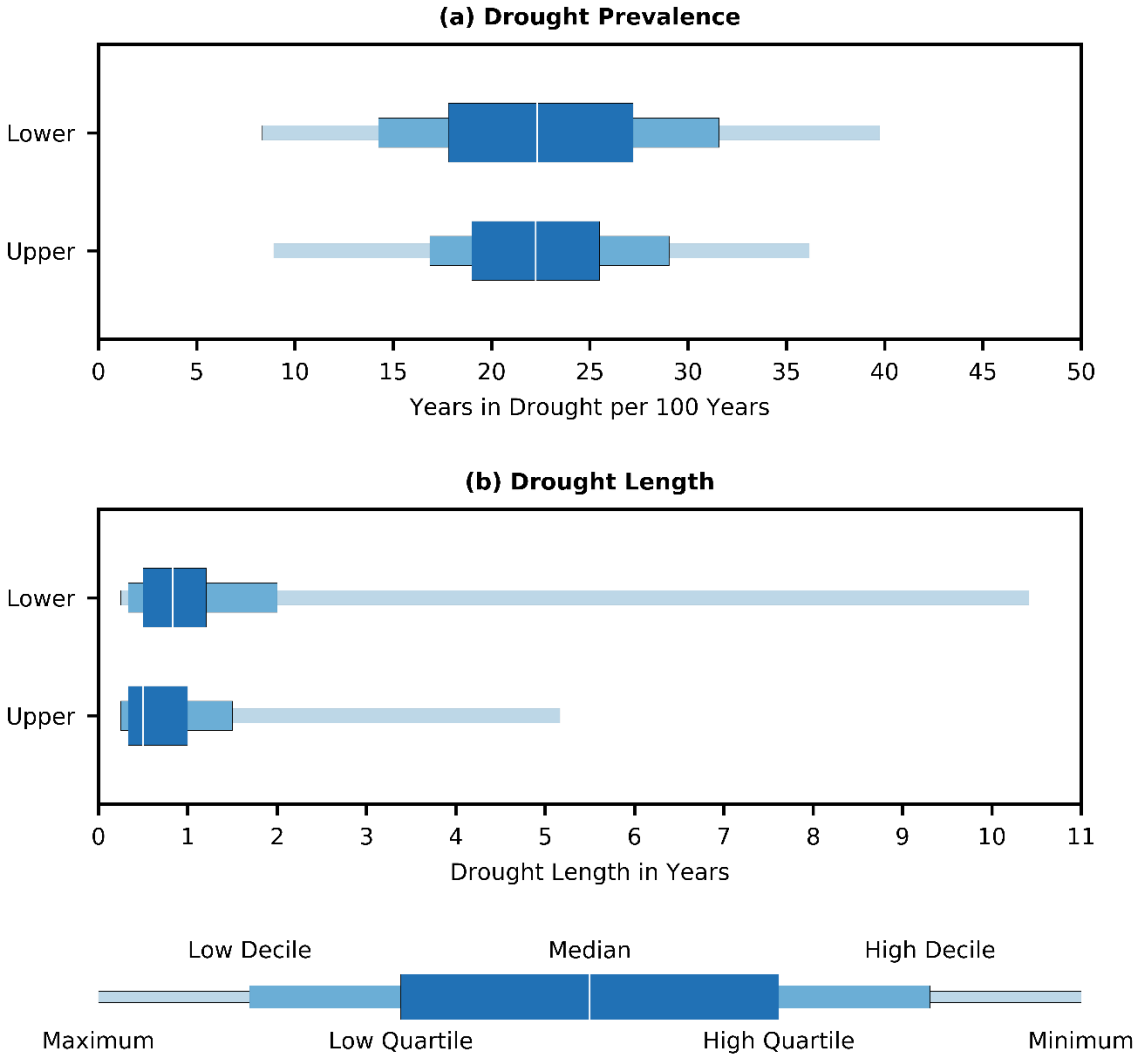

Figure 9: Box plots of (a) drought prevalence in years and (b) drought length in years based on the 40 CESM realizations in the Upper and Lower Amu Darya regions.

936

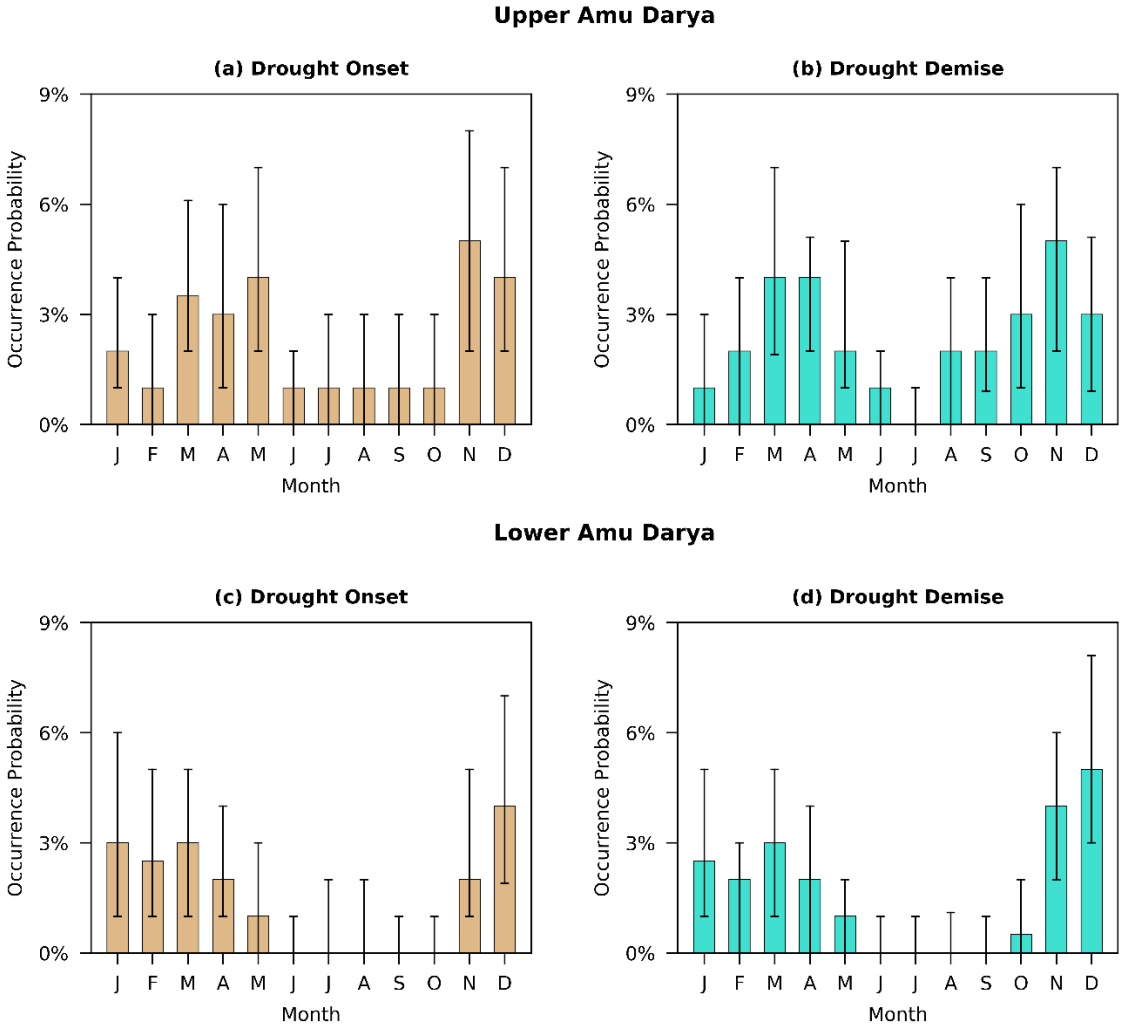

Figure 10: Monthly occurrence of drought (left column) onset and (right column) demise in the (top row) Upper and (bottom row) Lower Amu Darya regions. The bars represent the median occurrence and the whiskers the interdecile range. The median and the deciles are obtained from the drought occurrence across each of the 40 100-year CESM realizations.

937

938

939

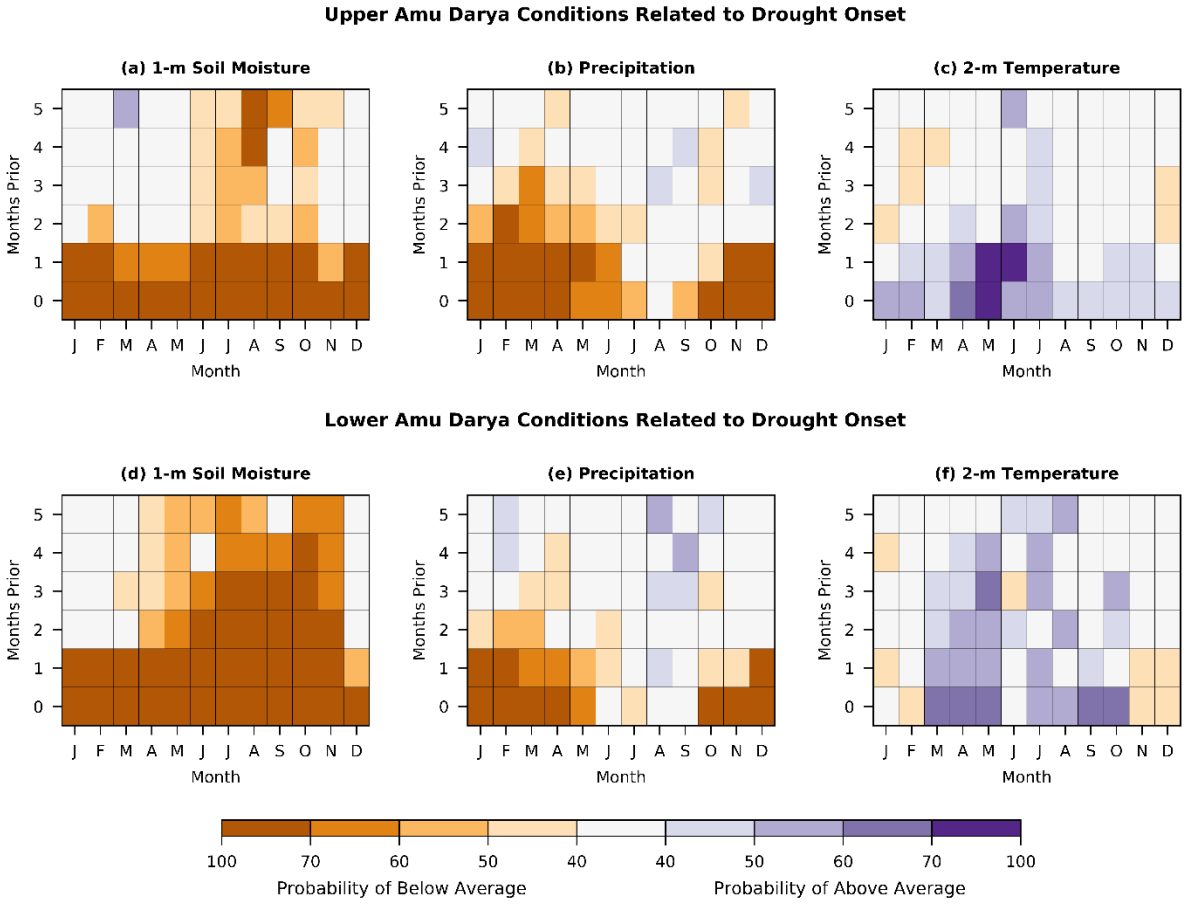

Figure 11: The probability of above or below average (left column) 1-m soil moisture, (center column) precipitation and (right column) 2-m air temperature for the (top row) Upper and (bottom row) Lower Amu Darya regions related to drought onset in the CESM realizations. 0 months prior indicates the month of drought onset and 5 months prior indicates five months prior to drought onset. The most likely category is plotted when it exceeds 40%.

940

941

942

943

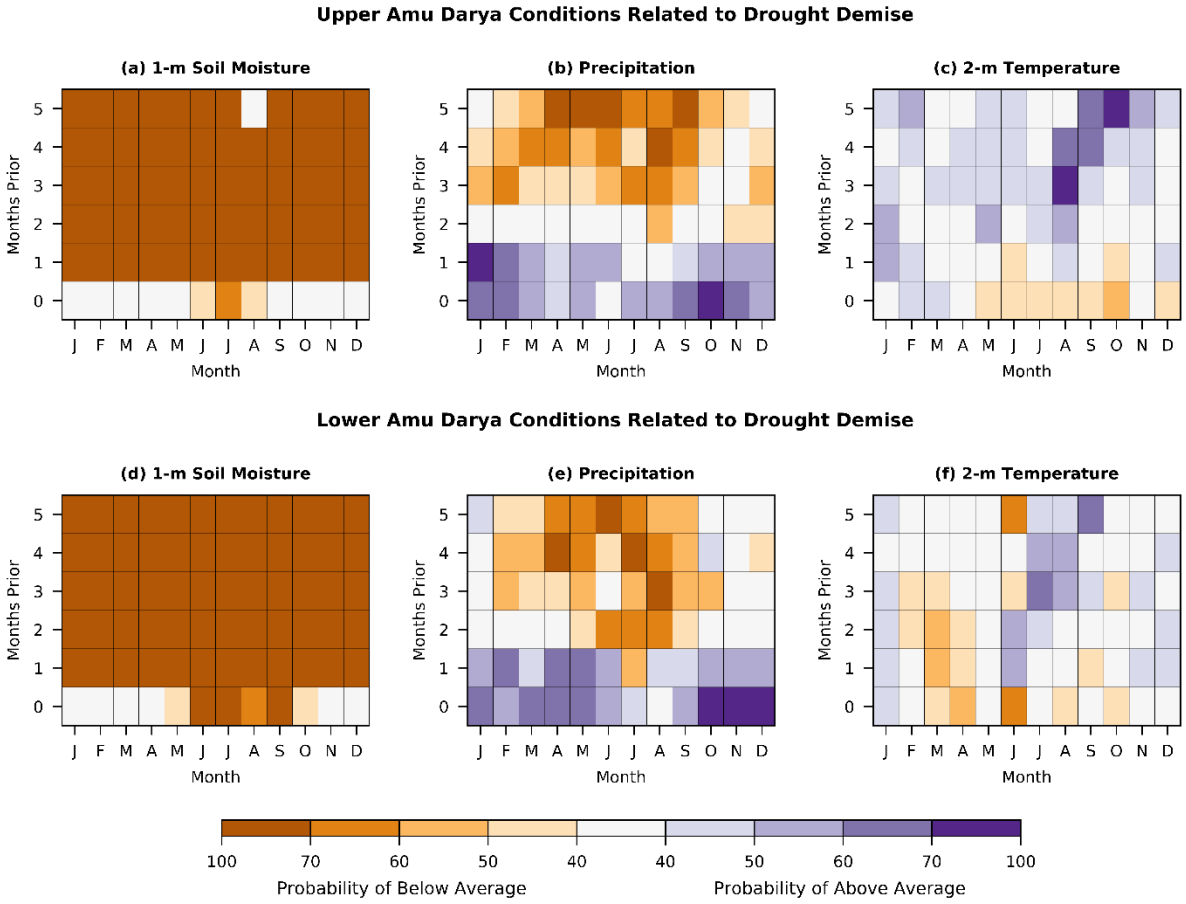

Figure 12: The probability of above or below average (left column) 1-m soil moisture, (center column) precipitation and (right column) 2-m air temperature for the (top row) Upper and (bottom row) Lower Amu Darya regions related to drought demise in the CESM realizations. 0 months prior indicates the month of drought demise and 5 months prior indicates five months prior to drought demise. The most likely category is plotted when it exceeds 40%.

944

945

946

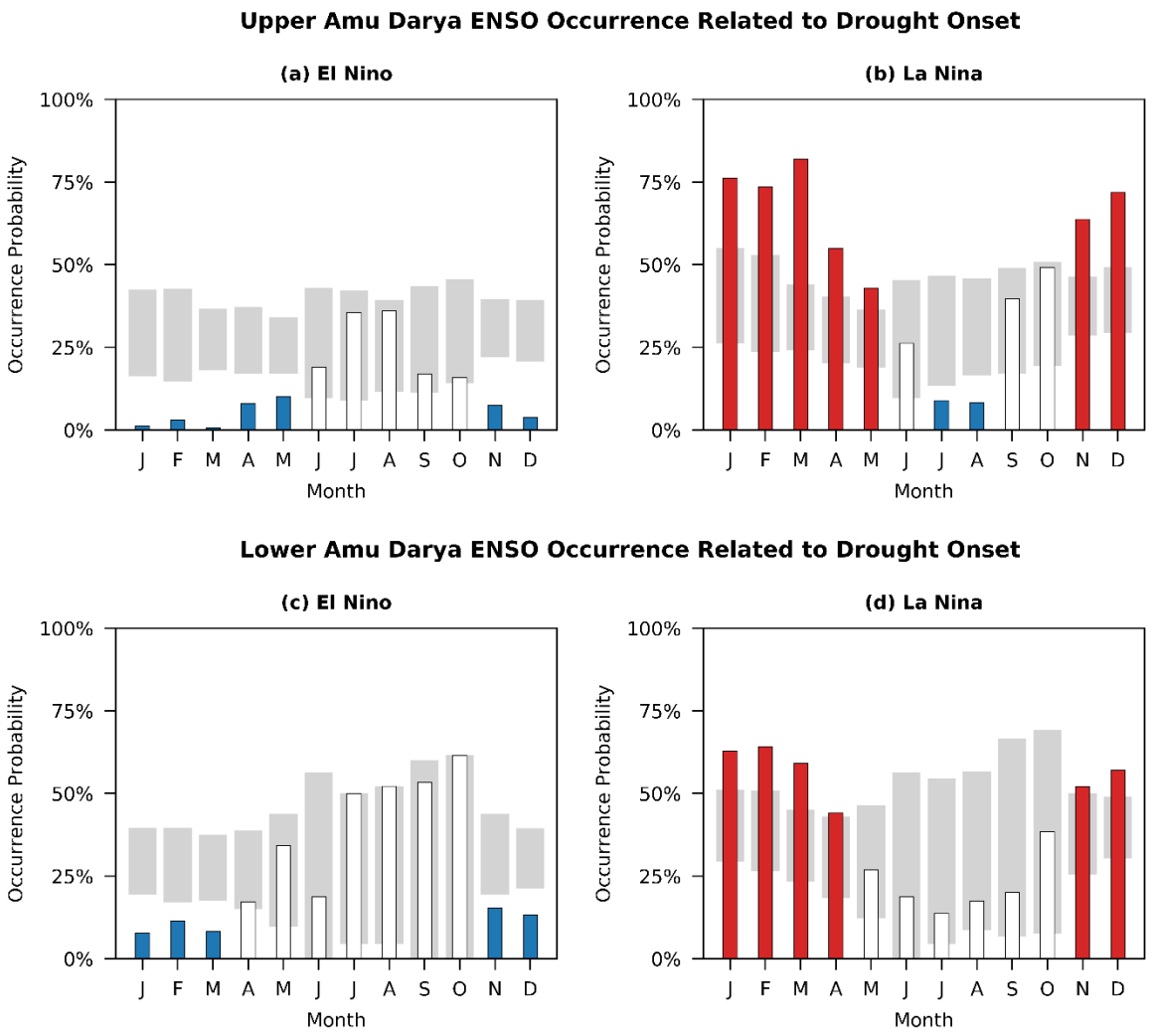

Figure 13: Occurrence of El Niño (left column) and (right column) La Niña in the (top row) Upper and (bottom row) Lower Amu Darya regions related to drought onset in the CESM realizations. Red (blue) bars indicate statistically significant increases (decreases) in occurrence at $p<0.05$ based on resampling. The gray shading indicates the range of values at $p>0.05$. El Niño and La Niña occur when the Niño3.4 index exceeds 0.5°C and -0.5°C, respectively. The Niño3.4 index is defined as the area averaged SST anomaly over the region 5°S-5°N, 170°W-120°W.

947

948

949

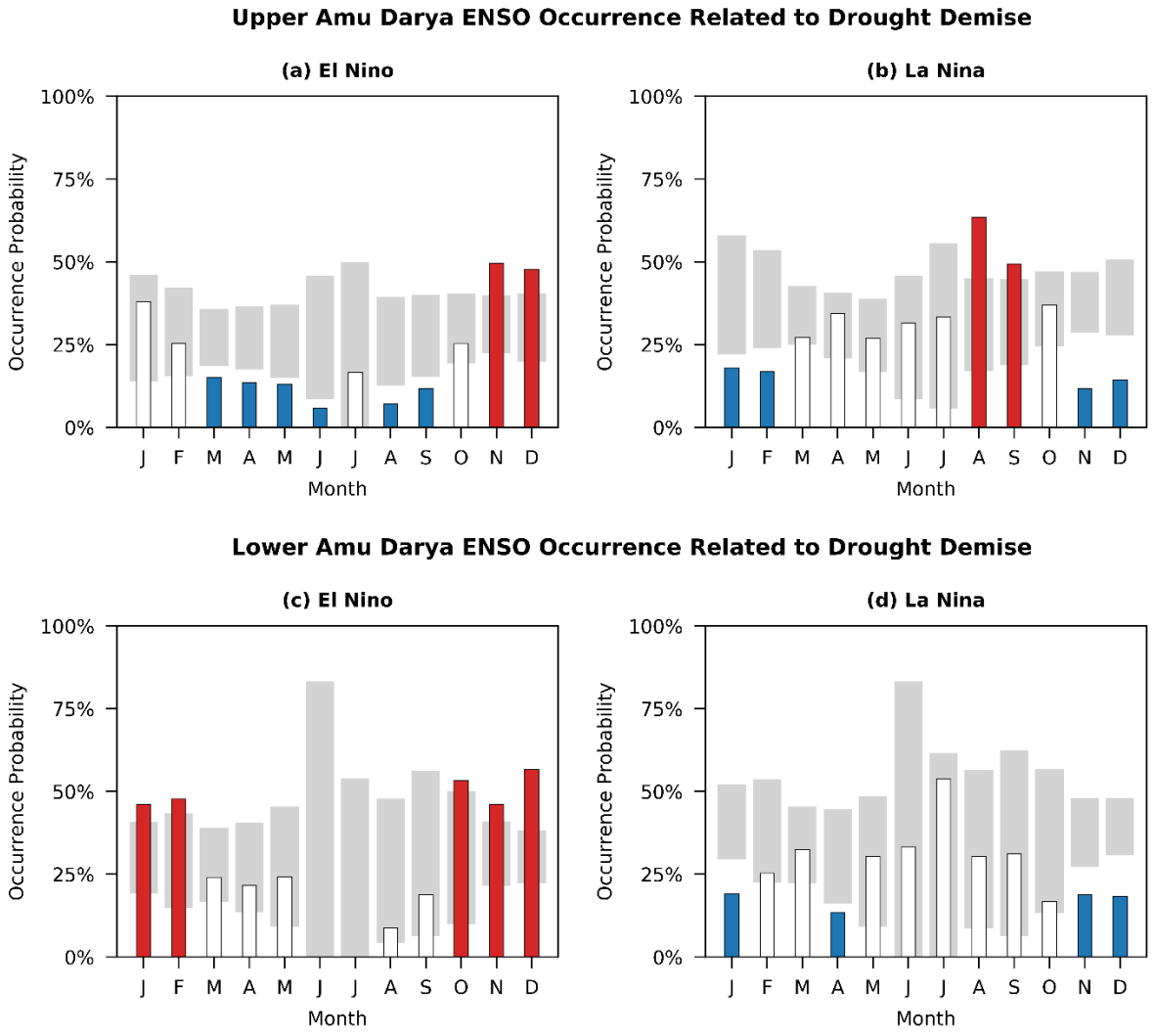

Figure 14: Occurrence of El Niño (left column) and (right column) La Niña in the (top row) Upper and (bottom row) Lower Amu Darya regions related to drought demise in the CESM realizations. Red (blue) bars indicate statistically significant increases (decreases) in occurrence at $p<0.05$ based on resampling. The gray shading indicates the range of values at $p>0.05$. El Niño and La Niña occur when the Niño3.4 index exceeds 0.5°C and -0.5°C, respectively. The Niño3.4 index is defined as the area averaged SST anomaly over the region 5°S-5°N, 170°W-120°W.

950

951

952

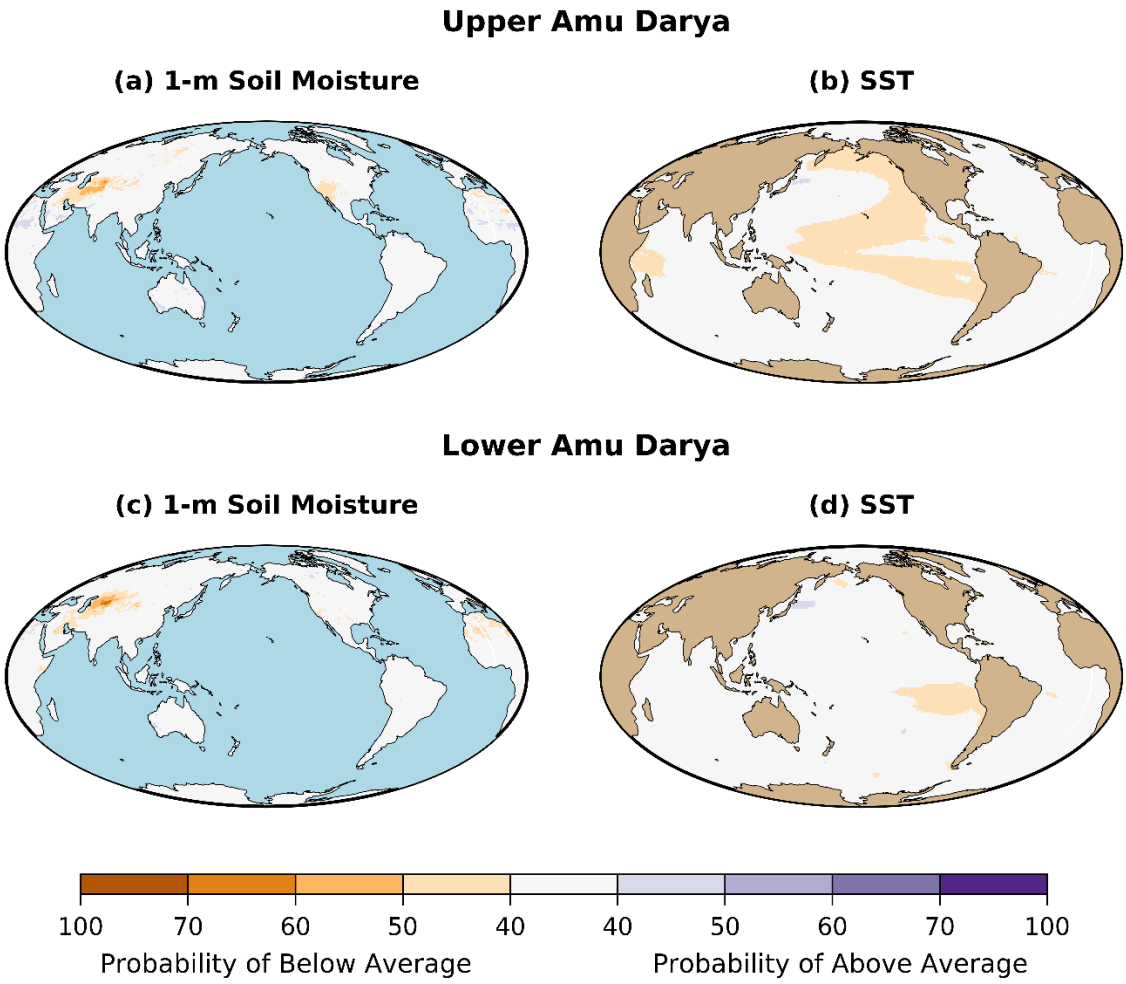

Figure 15: The probability of above or below average (left column) 1-m soil moisture and (right column) SST for the (top row) Upper and (bottom row) Lower Amu Darya regions during 10-year periods in which drought was most prevalent in the CESM realizations. The most likely category is plotted when it exceeds 40%. Most prevalent drought decades are defined as the top decile of drought occurrence in non-overlapping 120-month periods.

953